Journal of Asian Earth Sciences 229 (2022) 105179

Contents lists available at ScienceDirect

Journal of Asian Earth Sciences

journal homepage: www.elsevier.com/locate/jseaes

Late Holocene hydroclimatic changes inferred from a karst peat archive in the western Guizhou Plateau, SW China

Mengxiu Zeng [a], Qiao Zeng [a], Haijun Peng [b,*], Yongqiu Wu [a,*], Yue Li [c], Yougui Song [c], Enguo Sheng [d], Yangyang Wu [e], Tianyang Wang [a], Jian Ni [f]

[a] College of Geography and Environmental Sciences, Zhejiang Normal University, Jinhua 321004, China
[b] State Key Laboratory of Environmental Geochemistry, Institute of Geochemistry, Chinese Academy of Sciences, Guiyang 550081, China
[c] State Key Laboratory of Loess and Quaternary Geology, Institute of Earth Environment, Chinese Academy of Sciences, Xi'an 710061, China
[d] College of Resources and Environment, Zunyi Normal College, Zunyi 563002, China
[e] School of Geography and Resources, Guizhou Education University, Guiyang 550018, China
[f] College of Chemistry and Life Sciences, Zhejiang Normal University, Jinhua 321004, China

ARTICLE INFO

Keywords:
Ca-related indices
Medieval Warm Period
Little Ice Age
SW China
Karst region

ABSTRACT

The paleoenvironmental implications of Ca-related indices of peat from karst regions are poorly understood. In this study, we analyze a 450-cm peat core drilled from a sub-alpine karst mountain in the western Guizhou Plateau, SW China. This core is analyzed for carbonate contents and loss on ignition (LOI). High-resolution X-ray fluorescence (XRF) core scanning was also performed to see the variation of chemical compositions. Based on these measurements and 12 accelerator mass spectrometry (AMS)^{14}C dates, we reconstructed the history of hydroclimatic shifts in SW China and explored the significance of Ca-related indices. The reconstructed hydroclimatic conditions were consistent with the stalagmite, lacustrine sediment, and peat records from the regions controlled by the Indian monsoon. Abrupt decreases in precipitation and temperature were clearly shown during the 4.2 ka and Little Ice Age (LIA) cold events. High carbonate contents in the Yejiping peat during the Medieval Warm Period (MWP) were linked to a warm and humid climate. Additionally, wavelet analysis shows that variations in Ca content have 500, 125, 103, 80, 58, 43, 20, and 12-a quasi-periods, which correspond to the Gleissberg, Pacific Decadal Oscillation (PDO), and Schwabe cycles. Our results highlight the importance of Ca-related indices in peat deposits from karst depressions and provide a detailed description of the MWP and the LIA.

1. Introduction

Carbonate contents of terrestrial sediments are widely used to decipher paleoclimatic variations, but interpretations based on such contents differ according to the differences in carriers (Chen et al., 2007; Fan et al., 2019). Many studies in loess-paleosol sequences have suggested that changes in carbonate contents can reveal the paleoclimatic evolution processes (Chen et al., 2007; Fang et al., 1994; Lu, 1981). For example, increases in carbonate contents were usually used as indicators of dry climate (Han et al., 1997; Hans, 1980). Higher percentages of carbonate minerals denoted a decrease in precipitation and runoff; thus, they have been used to indicate the hydrological balance of Lake Dali (Fan et al., 2019). It has been reported that the carbonate contents of the sediments from Lake Lugu and Lake Qilu are mainly controlled by lake water level changes (Hillman et al., 2020; Zheng et al., 2014). However, the environmental significance of Ca-related indices varies with the surrounding environment of the catchment area. For example, higher concentrations of calcite in sediments from Lake Ontario, Lake Seneca, and Lake Cayuga were found to correspond to warmer and wetter climates (Silliman et al., 1996; Anderson and Mullins, 1997; Mullins, 1998). These studies show that carbonate contents of lacustrine sediments have different environmental implications in different regions. However, studies on peat archive study from regions with widespread carbonate rocks are scarce.

Karst landforms and carbonates are widely distributed across southwestern China, with Guizhou having the largest karst topography at the provincial level, making it an ideal place for studying the hydroclimatic implications of carbonate content in paleoenvironmental

* Corresponding authors.
E-mail addresses: penghaijun@mail.gyig.ac.cn (H. Peng), wuyongqiu@zjnu.edu.cn (Y. Wu).

https://doi.org/10.1016/j.jseaes.2022.105179
Received 27 July 2021; Received in revised form 26 February 2022; Accepted 28 February 2022
Available online 3 March 2022

carriers, such as peat. Studies on the paleoclimate evolution of this region have been extensively carried out and have revealed frequent and abrupt climatic changes during the late Holocene in Guizhou (Dykoski et al., 2005; Gao et al., 2019; Niu et al., 2017). For example, the abrupt cooling events in ~4200 and ~1100–900 cal. a BP were widely recorded in stalagmite, peat, and lacustrine sediments (Gong et al., 2019; Quan et al., 2019; Dykoski et al., 2005; Niu et al., 2017; Zhang et al., 2009). It has been suggested that there were several stages of climatic fluctuations during the Little Ice Age (LIA, 1450–1850 CE, IPCC Fifth Assessment Report), which is the last cold event over the past 1000 years (Zhang et al., 2006; Zhang et al., 2009; Zhao et al., 2015a). Owing to differences in temporal resolution, dating methods, and local geological background, the duration of these cold sub-periods during the LIA varies slightly among different study sites (Yu et al., 2020; Zhang et al., 2009; Zhao et al., 2015b). Mostly, ~2–3 distinct cold sub-periods can be clearly identified, suggesting obvious cold-warm and dry-wet fluctuations during the LIA. These records were mainly derived from cave stalagmites and lake sediment cores, while studies into peat records in SW China are still scarce.

Multi-proxy-based global paleoclimate records from various carriers have recorded the abrupt changes during the Medieval Warm Period (MWP, 950–1450 CE according to the IPCC Fifth Assessment Report). Peat has been considered as an ideal carrier for paleoclimate reconstructions (Lopez-Aviles et al., 2021; Mikhailova et al., 2021; Nazarova et al., 2021; Njagi et al., 2021; Sachs et al., 2021), just as lacustrine sediments (Quamar and Bera, 2021; Wang et al., 2021a; Wang et al., 2021b), cave stalagmites (Chen et al., 2021), ice cores (Grieman et al., 2018), tree rings (Hadad et al., 2021), aeolian sediments (Bhattacharya et al., 2017), and coastal deposits (Manoj et al., 2021). Previous studies have shown that the MWP lasted from 850 to 1350 CE, from 940 to 1220 CE, from 750 to 1200 CE, from 650 to 1350 CE, from 700 to 1250 CE, from 760 to 1325 CE, and from 900 to 1250 CE in southwestern China (Feng et al., 2019; Wang et al., 2021a), central India (Tripathi et al., 2021), northeast India (Quamar and Bera, 2021), Mongolia (Rudaya et al., 2021), East Russia (Nazarova et al., 2021), East Africa (Njagi et al., 2021), and the central equatorial North Pacific (Sachs et al., 2021), respectively. Carbon isotope ratios ($\delta^{13}C$) of stalagmites from Shijiangjun Cave in Guizhou Province revealed dry climate conditions during the MWP (Chen et al., 2021). Mineral records in the sediments from Lake Ayakum on the northern margin of the Qinghai-Tibet Plateau (QTP) (Wang et al., 2021b) and Lugu Lake in northwestern Yunnan (Wang et al., 2021a) also showed a dry MWP. Besides, a dry MWP has been recorded in East Africa (Njagi et al., 2021), South America (Hadad et al., 2021), southern Iberian Peninsula (Lopez-Aviles et al., 2021), Mongolia (Rudaya et al., 2021), and central equatorial North Pacific (Sachs et al., 2021). Contrastingly, a wet MWP was recorded in southern East Siberia (Mikhailova et al., 2021), East Russia (Nazarova et al., 2021), Mediterranean (Kaniewski et al., 2011), and the Indian subcontinent (Dixit and Tandon, 2016; Manoj et al., 2021; Quamar and Bera, 2021; Tripathi et al., 2021). These contradictions demonstrate there is still no consensus about the exact timing of the MWP due to chronological uncertainty, sampling resolution, etc. Furthermore, compared with the LIA, there are fewer MWP records in Guizhou, large uncertainties remained in the understanding of the climate during this period in Guizhou.

Ca and $CaCO_3$ contents have been widely used to reconstruct changes in the environment in different geological backgrounds (Zheng et al., 2014). However, such studies are rare for peat deposits, especially in karst areas where the bedrock weathering is sensitive to climate changes. Several studies have been conducted on peat records in and around China, but very few have been conducted in Guizhou (Cui et al., 2018). Additionally, previous studies were concentrated on reconstructing the overall climatic changes during the Holocene (Wang et al., 2010), the climate fluctuations during specific periods like the LIA and MWP are still understudied. In this study, we analyzed a 450-cm-long peat core (YJP01) that was taken from Yejiping, an ombrotrophic peatland in the western Guizhou Plateau in SW China. This peatland, with no river input from its surface and surroundings, is developed on and surrounded by carbonate rocks. We conducted X-ray fluorescence (XRF) core scanning, loss on ignition (LOI), carbonate content, dry density, and extensive AMS^{14}C measurements on the core YJP01. The objectives of this study are to (1) reveal the climatic and environmental significance of Ca-related indices in karst peat core; (2) reconstruct high-resolution climatic changes in the Indian monsoon-dominated region during the MWP and LIA; and (3) investigate the driving forces of climate variations in SW China since the late stage of the middle Holocene.

2. Study area

The YJP01 peat core was retrieved from the Yejiping alpine peatland (26.45°N, 104.697°E, 2241 m a.s.l.), which is located close to the junction of the Guizhou and Yunnan Provinces in SW China (Fig. 1A, B). This peatland is in a low-lying terrain in the Wumeng mountains, which lies 19 km to the southwest of Shuicheng County, Liupanshui City, in the west of Guizhou Plateau (Fig. 1B, C, D). The Yejiping peatland is surrounded by karst landforms and is devoid of rivers. The average elevation of Shuicheng County, which is located in the Wumeng Mountains, is about 1700–1800 m. Karst landforms accounted for 63.18% of the total area of the Liupanshui City (Deng and Bi, 2004). The outcrop lithology of this area mainly consists of Permian limestone (P1) intercalated with dolomite and sandy shale, Carboniferous limestone (C2) and dolomite (sandy shale in the upper part is intercalated with argillaceous limestone). The lower part of C2 is composed of limestone interposed with shale, sandy shale with coal or aluminous phases, while limestone and dolomite dominate the upper part (Fig. 1B) (Dai et al., 2014; Li, 2001).

The climate of Liupanshui City is humid-subtropical-mountainous that greatly affected by the Indian monsoon (Zheng et al., 2013; Zhang and Wu, 2020) (Fig. 1A). Rainfall in the Liupanshui region mainly occurs from May to September, accounting for 71–88% of the annual precipitation. The average annual temperature and average annual precipitation are 15 °C and 1200 mm, respectively. The rivers in the Wumeng Mountains are part of the middle reaches of the Beipan and the Redu River systems, which finally flow into the Pearl River (Fig. 1C). The typical vegetation in this region includes mountain evergreen oak forests, Yunnan pine forests, and walnut forests (Huang and Tu, 1983). Located in the watershed between the Wujiang and Beipanjiang river, Shuicheng County is known as the “plateau pearl” of Guizhou Province. Besides, Shuicheng County has also been recognized as a very important area for the coal industry in SW China.

3. Materials and methods

3.1. Sampling

The YJP01 peat core was drilled from the center of the Yejiping peatland using a Russian peat corer (Fig. 1C, D). The depth of YJP01 is 450 cm. The collected samples were immediately packed in 50 cm-long polymethyl methacrylate half-cylinder tubes and transported back to the laboratory. The cores were then stored in a refrigerator at 4 °C until they were sliced into 1-cm sub-samples. From the top to the bottom, the lithological (Fig. 2B) descriptions are listed below:

① 0–20 cm is mainly composed of yellow–brown peat. The surface layer contains a lot of macroscopic live plant roots with a small number of woody debris.
② 20–50 cm is brown-black peat containing many undecomposed plant residues.
③ 50–200 cm is well compacted and decomposed dark black peat with few plant residues.

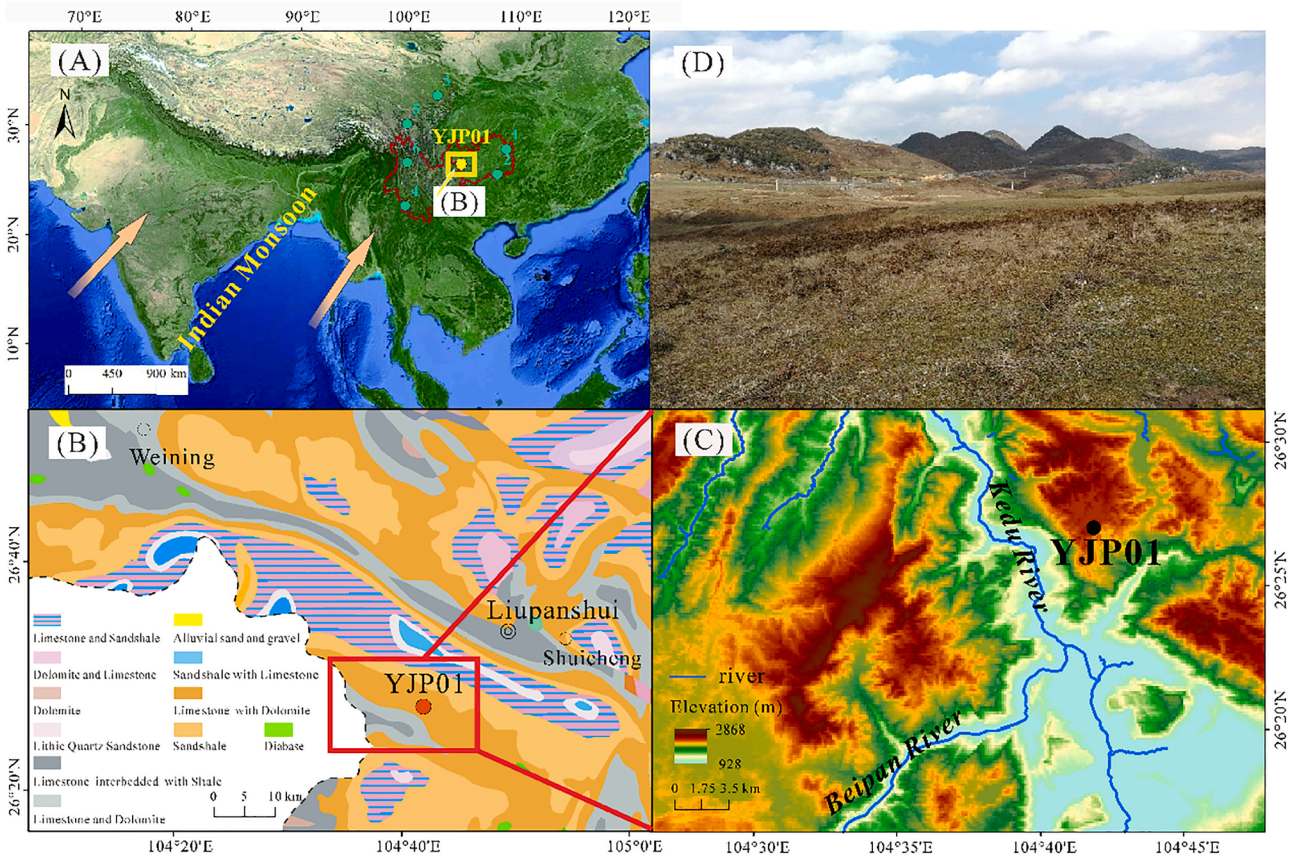

Fig. 1. Natural background of the study area and the sampling site. (A) Geographic and climatological locations of the Yejiping peatland, and the relevant paleoclimate records: 1- Lake Jiulongchi (Gao et al., 2019), 2- Dongge Cave (Dykoski et al., 2005; Wang et al., 2005), 3- Hongyuan Peat (Yan et al., 2021), 4- Lake XMLT (Ning et al., 2017), 5- Lake Ruogen Co (Ming et al., 2020), and 6- Lake Tiancai (Xiao et al., 2014), YJP01- this study, (B) large scale geological map showing the stratigraphy across northwestern Guizhou (Dai et al., 2014; Li, 2001), (C) structural setting and elevation background of Yejiping peatland and the location of the YJP01 core, and (D) field photo of Yejiping peatland.

④ 200–285 cm is brown peat containing undecomposed plant rhizomes and sphagnum moss. This part is porous, and its water content is high.
⑤ 285–385 cm is highly decomposed black peat that has few plant rhizomes and woody debris.
⑥ 385–420 cm is firm and highly decomposed gray peat with no plant residue observed.
⑦ 420–450 cm is gray-brown peat mixed with a small amount of fine-grained gravel and a few microscopic plant residues.

3.2. Methods

3.2.1. Dating and age–depth model

Based on the above-mentioned depositional characteristics of the YJP01 core, 12 plant residue samples were selected for the accelerator mass spectrometry (AMS) ^{14}C dating (Fig. 2A, B). The AMS ^{14}C measurements were conducted at Beta Analytic. The IntCal13 curve was used to calibrate the AMS measurements by the OxCal program. The Bacon 2.2 R package (Blaauw and Christen, 2011), which is based on Bayesian statistical methods, was used to establish the age-depth model (Fig. 2C).

3.2.2. High-resolution XRF core scanning

XRF core scanning was carried out at the State Key Laboratory of Lakes and the Environment, Nanjing Institute of Geography and Limnology, Chinese Academy of Sciences, using a high-resolution multi-parameter core scanner (MSCL, GeoTek Ltd., UK). After lithology inspections and high-resolution photography, continuous XRF element measured at 1 cm resolution were carried out on the YJP01 core. Mg, Ca, Fe, and other elements contents were measured at the voltage of 10 keV for a 10-second count time. Brightness (L*), redness (a*), and yellowness (b*) were also obtained at 1 cm intervals. The element signal intensities of the XRF scans were expressed as peak areas in counts per second (cps). Due to high TOC content, Al contents were used to calibrate the XRF scanning results following the suggestions in previous studies (Löwemark et al., 2011; Yang et al., 2019). The element contents become dimensionless after the calibration. Ca/Al ratios were used to represent in the subsequent figures, but Ca is still used in the text.

3.2.3. Measurements of LOI and carbonate contents

Samples in each core pillar were sub-divided into 1-cm intervals, and a total of 450 samples were obtained and then stored in self-sealed bags. Organic matter and carbonate contents were determined using the combustion method. First, the empty corundum crucibles were heated in a muffle furnace at 550 °C for 4 h and then cooled to room temperature in a desiccator to maintain a constant weight. The net weight of the crucible was then measured. Second, the samples were placed into small containers with a volume of 4.096 cm^3 and oven-dried at a constant temperature of 105 °C for 12 h. The wet weight and dry weight were measured, and then both the water content and dry density of the samples were calculated (van Bellen et al., 2011). The samples were put in the dried corundum crucibles and calcined at 550 °C for 4 h in a muffle furnace, and then weighed. The LOI of each sample was then calculated. After performing the LOI measurements, the samples were again placed in a muffle furnace and calcined at 950 °C for 4 h. After being cooled to room temperature in a desiccator, the crucibles were

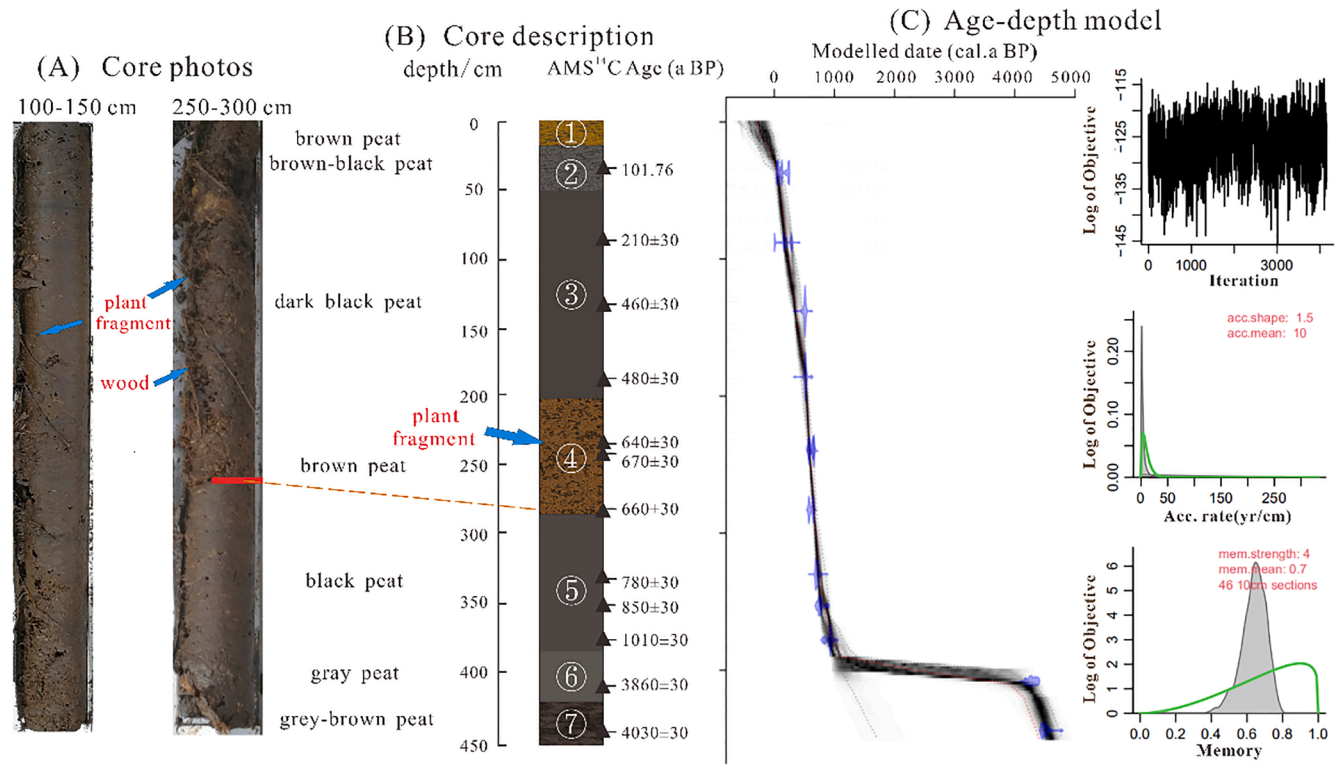

Fig. 2. Study materials and the age-depth model of the YJP01. (A) Core photos of the YJP01, (B) stratigraphy and AMS ^{14}C dates from the YJP01 core, (C) age–depth model created using the Bacon 2.2 R package. In figure (C), the upper right plot shows the stability of the Markov Chain Monte Carlo iterations (>1000 iterations), the middle plot shows the prior (green curve) and posterior (gray fill) dependences for the accumulation rates (a/cm), and the lower right plot shows the prior (green curve) and posterior (gray fill) dependences of accumulation rates between piece-wise sections. (For interpretation of the references to color in this figure legend, the reader is referred to the web version of this article.)

weighed again and then calculated for carbonate contents (hereafter referred as $CaCO_3$) (Shi et al., 2021).

3.2.4. Scanning electron microscopy (SEM) analysis

Four samples were selected for SEM micromorphology analysis. The organic matter in the samples was first removed using the excess hydrogen peroxide method. The samples were then freeze-dried and fixed with conductive carbon tape and gold-plated. The extracted samples were then observed using a Feiner desktop SEM (PhenomTM proX, energy spectrum version). A full image of each sample was taken by the SEM system. Sample preparation and SEM analyses were performed at the Institute of Earth Environment, Chinese Academy of Sciences.

3.2.5. Multivariate statistical analysis

The Morlet wavelet transform function was used to analyze the cycles in the Ca content. The analysis was done using the MATLAB R2016a software (The Mathworks Ltd, USA). Additionally, power spectrum analysis was performed using the free software Past3 (https://www.nhm.uio.no/english/research/infrastructure/past/). The power spectrum results were tested at both 80% and 90% confidence intervals.

4. Results

4.1. Chronology and deposition dynamics

The AMS^{14}C chronology results of the YJP01 core (Table 1) showed that there were no age reversals across the depth range of 0–392 cm (after 1140 cal. a BP). The sedimentation rate was relatively stable in this section, with an average value of 3.7 mm/a. The sample at 15 cm depth is dated to be 1960 CE. There might exist a sedimentary hiatus at 392–393 cm, but the cause is still not clear. The average sedimentation rate at 394–450 cm was ~0.73 mm/a. According to the age-depth model, which has 2 age control points in the section from 394 to 450 cm, the age at the bottom of the core (450 cm) was 4732 cal. a BP

Table 1
AMS radiocarbon dating results from the YJP1 profile.

Lab. code	Sam. code	Depth (cm)	Dated material	δ^{13}C (‰)	^{14}C Age (a BP)	Calibrated age range a BP (2σ, %)
Beta-560262	YJP18-1–37	36.5	Plant fragment	−28.3	101.76 ± 0.38 pMC	54 ± 17 (34)
Beta-560263	YJP18-2–38	87.5	Plant fragment	−26.2	210 ± 30	182 ± 39 (55)
Beta-552193	YJP18-3–38	137.5	Plant fragment	−26	460 ± 30	509 ± 29 (100)
Beta-560264	YJP18-4–36	185.5	Plant fragment	−24.6	480 ± 30	519 ± 23 (100)
Beta-552194	YJP18-5–38	237.5	Plant fragment	−22.7	640 ± 30	584 ± 30 (57)
Beta-560265	YJP18-5–40	239.5	Plant fragment	−23.5	670 ± 30	650 ± 22 (55)
Beta-560266	YJP18-6–33	282.5	Plant fragment	−27.9	660 ± 30	648 ± 23 (51)
Beta-560267	YJP18-7–30	329.5	Plant fragment	−24.7	780 ± 30	701 ± 30 (100)
Beta-569154	YJP18-353	352.5	Plant fragment	−28.2	850 ± 30	739 ± 55 (99)
Beta-569153	YJP18-378	377.5	Plant fragment	−27.3	1010 ± 30	930 ± 29 (74)
Beta-552195	YJP18-9–8	408.5	Wood	−24.2	3860 ± 30	4318 ± 90 (84)
Beta-560268	YJP18-9–44	443.5	Plant fragment	−24.5	4030 ± 30	4497 ± 77 (100)

(Fig. 2C).

4.2. Results of high-resolution XRF core scanning

Ca content varied from 2.216 to 26.95 after the calibration, while Mg content varied from 0.04 to 1.03 (average 0.513) throughout the peat core. The correlation coefficient (R) between Ca and Mg was 0.967 ($P < 0.01$, n = 449). Fe_2O_3 ranged from 53 to 6319 (average 1804.64) and was significantly negatively correlated with Ca and Mg (R = -0.753 and −0.751, respectively; P < 0.001, n = 449). a* was significantly positively correlated with b* (R = 0.850, $P < 0.001$, n = 449) (Fig. 3F, G), whereas a* and b* were negatively correlated with L* (R = −0.258 and −0.501, respectively, $P < 0.001$, n = 449). L* varied from 4.69 to 55.14 (average 34.43). Ca content exhibited an overall increasing trend from the bottom to the top of the core (Fig. 3).

4.3. Carbonate content and LOI

Both $CaCO_3$ (ranging from 0.018 to 6.42%, average 2.12%) and LOI (ranging from 8.4 to 83.97%, average 46.58%) showed an overall increasing trend from the bottom to the top of the core (Fig. 3). Some clay layers and small amounts of fine gravel were observed in the section at 450–420 cm depth (Fig. 2). Besides, both $CaCO_3$ and LOI of this section are very low, this is probably related to the fact that it was at the early stage of peat development. Furthermore, both $CaCO_3$ and LOI have obviously increased in the section at 420–385 cm depth. The section from 385 to 285 cm had relatively high $CaCO_3$ and LOI values (Fig. 3). From 285 to 200 cm depth, the sediments composed brown peat rich in plant residue, and $CaCO_3$ and LOI reached their maximum values. From 200 to 50 cm depth, both $CaCO_3$ and LOI fluctuated significantly and had relatively low values. The peat above 50 cm was composed brown-black peat and showed increases in both $CaCO_3$ and LOI. High $CaCO_3$ and LOI generally denoted high Ca and L*. Ca was significantly positively correlated with LOI (R = 0.526, $P < 0.001$, n = 449) and $CaCO_3$ (R = 0.35, $P < 0.001$, n = 449). Peat with high LOI and $CaCO_3$ (or Ca) had a lighter color and thus had a higher L*.

4.4. Morphological characteristics of the peat debris

The debris from different depths was clearly shown in the SEM graphs and they are morphologically different (Fig. 4). With the increase in depth, these debris have experienced stronger weathering, erosion, and corrosion. These debris were angular to sub-rounded, while well-rounded grains were not observed. The particle size of the detrital minerals at depths of 410 and 366 cm was smaller than the shallower ones. At the depth of 149 cm, the size of detrital minerals remained the same, but angular grains became abundant. Contrastingly, the grain size of the sample at 214 cm was larger and depicted a higher roundness (Fig. 4).

4.5. Cyclic variations in Ca contents

Power spectrum analysis of the Ca counts (Fig. 5A) showed significant quasi-periods of 500, 125, 103, 80, 58, 43, 38, 30, 27, 20, and 12a. In addition, wavelet spectral energy of the variations in Ca revealed that the 512–500, 250–200, 64–40, and 22a quasi-periods were the most significant (Fig. 5B). The 500a quasi-period was observed during 800–400 cal. a BP, while a 130–100a quasi-period appeared from 1000 to 160 cal. a BP. The 40–20a quasi-periodic signal appeared intermittently since 1000 cal. a BP. Meanwhile, the 12a quasi-periodic signal became more pronounced since 800 cal. a BP. The results of the power spectrum and wavelet analyses were comparable and consistent with each other.

5. Discussion

5.1. Paleoenvironmental significance of LOI and Ca-related indices in the Yejiping peat record

Besides organic matter content, LOI also includes contents of components such as crystal water and volatile compounds (Heiri et al., 2001). However, the proportion of these components is tiny in peat, which is largely composed of organic matter that formed through the accumulation and decomposition of dead plants. LOI has been widely

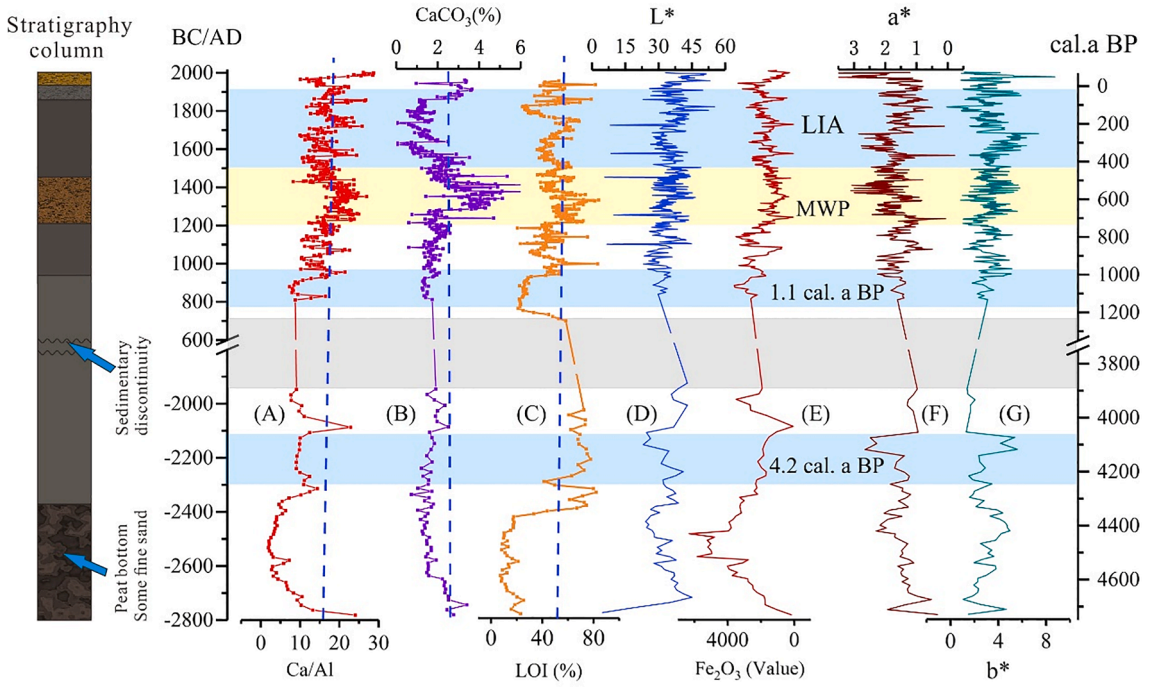

Fig. 3. Comparisons of Ca and $CaCO_3$ content compared with other records from the YJP01 core of the Yejiping peatland. (A) Ca, (B) $CaCO_3$, (C) LOI, (D) L*, (E) Fe_2O_3, (F) a*, and (G) b*. The gray shaded region indicates the hiatus part of this core.

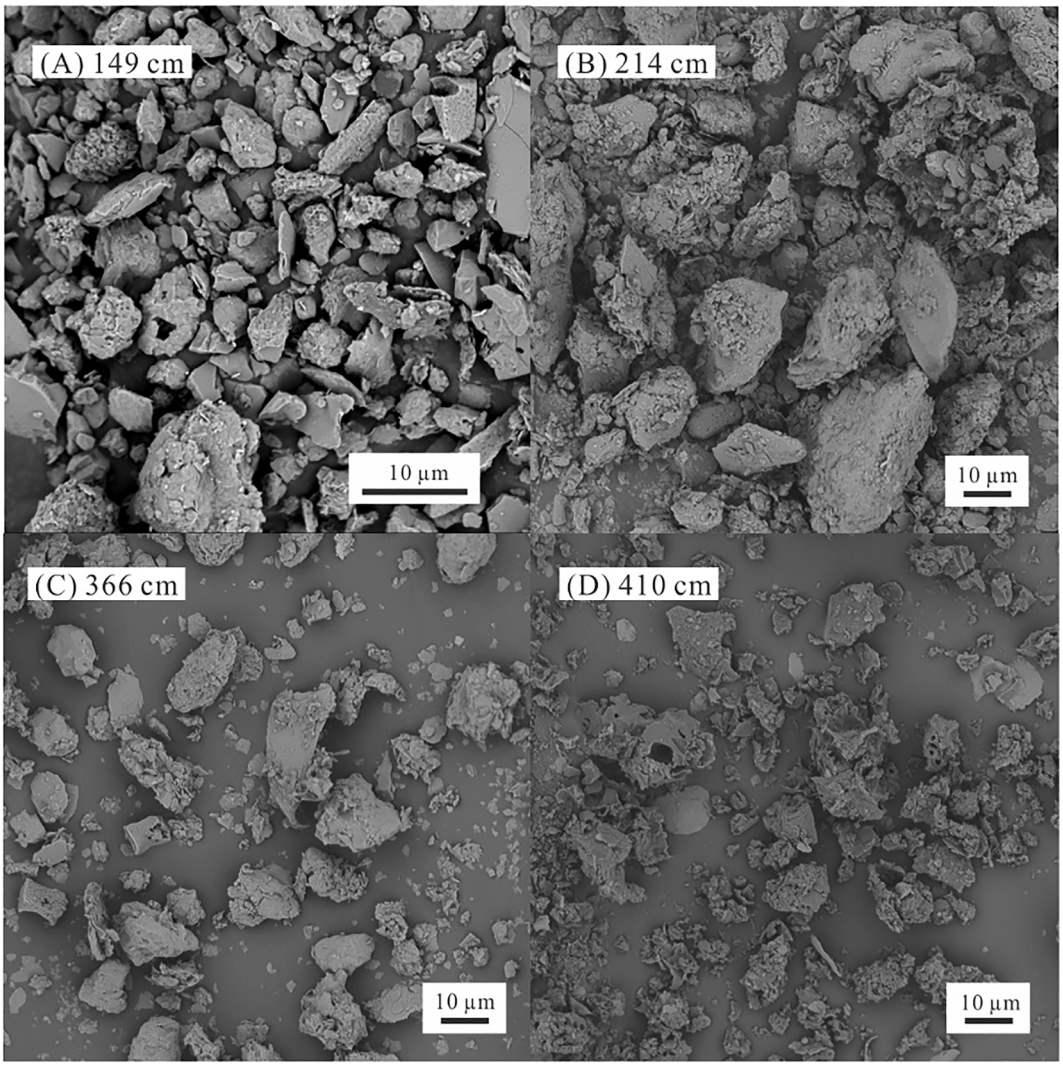

Fig. 4. Morphological characteristics of detrital mineral fraction under SEM from the YJP01 core of Yejiping peatland. (A) 149 cm from LIA, (B) 214 cm from MWP, (C) 366 cm at ~1000 cal. a BP and (D) 410 cm at ~4000 cal. a BP.

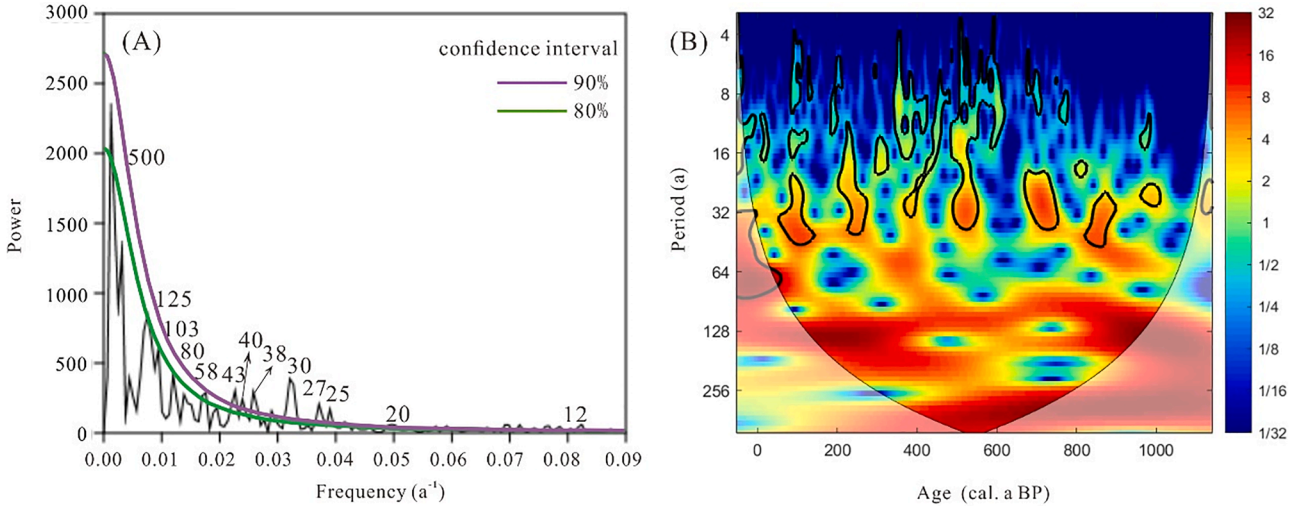

Fig. 5. Periods of the YJP01 core from the Yejiping peatland. (A) Power spectrum and (B) wavelet spectral energy (the black boundaries mark 90% significance level) for the Ca content of the YJP01 core.

used to calculate the variation in organic matter content in different sediments (Heiri et al., 2001; Konen et al., 2002; Cambardella et al., 2001). Variations in organic matter content can also reflect the primary productivity of peatland (Wu et al., 2011). As there is no major river flowing through the Yejiping peatland, organic matter in the peat mainly comes from indigenous plants in the peatland. The study area is mainly controlled by the Asian monsoon, and the productivity of the Yejiping peatland is strongly affected by temperature changes (Yang et al., 2020). This can be observed in the LOI variations of Yejiping peatland since 4700 cal. a BP (Fig. 6A), which shows significant periodical variations. The high temperature and monsoon precipitation were conducive to the plant growth during warm periods such as the MWP. The increases in organic matter content and LOI are in line with the increase in primary productivity in the Yejiping peatlands (Fig. 6A). Contrastingly, the organic matter content and LOI were low during cold periods, such as the LIA (Fig. 6A). The reconstructed mean annual temperature (MAT) at the Hongyuan Peatland (Yan et al., 2021), which is also controlled by the Indian monsoon, was relatively consistent with our LOI results (Fig. 6B). Besides, the variation in LOI of the YJP01 core was in line with the reconstructed MAT at Lake Kusai and Lake Lugu, which are in the north of the Qinghai-Tibet Plateau (QTP) and Yunnan Province, respectively (Fig. 6C and D) (Cui et al., 2021; Zhang et al., 2018; Zhao et al., 2020). The reconstructed summer (July) temperature of the Scandinavian Peninsula (Helama et al., 2012) (Fig. 6E) also showed a similar variation trend to the LOI of the YJP01 core, further revealing the influence of temperature on the LOI of the Yejiping peat.

Yejiping peatland is in a high elevation area rich in carbonate rocks, and the climate of this area has very strong seasonal variations. The high temporal resolution of the YJP01 core can aid in further understanding of the dynamics in Ca migration and leaching in peat records during the last millennium. Ca and Mg counts were significantly correlated throughout the YJP01 core ($R^2 = 0.97$, $P < 0.01$, n = 449). These similar geochemical properties can also be observed in other sediment records in karst regions, which can further explain the weathering process of the YJP01 core. It has been reported that the migration coefficients of Ca and Mg in the karst region of Guizhou are close to −1, meaning these elements are almost completely depleted (Zhang et al., 2015). Ca and Mg generally leach and migrate during the weathering process, which could then lead to the enriched CaO and MgO that were observed in the deposits in low-lying lands or lakes in karst regions, while their source areas were relatively depleted in CaO and MgO (Kong et al., 2011). For example, it has been suggested that the CaO enriched soil of Anlong Muzan, a montane valley, was mainly sourced from the surrounding karst mountains (Chen et al., 2010). Because of the weathering of carbonates is directly related to the intensity of precipitation, the Ca and Mg losses in the profile and stratum were proposed to be proportional to the amount of precipitation (Li et al., 2014). It is thus believed that the variations in the Ca contents of karst peat can efficiently record the precipitation intensities.

Peat always has a high organic content and is generally acidic, making it very different from lacustrine deposits (Chai, 1993). $CaCO_3$ is difficult to crystallize in acidic environments like the Yejiping peatland, and the calcium in the peat tends to be in an ionic state. In the Yejiping peatland, the runoff water and mineral material (Ca and other elements) are mainly derived from precipitation or surrounding weathering leaching. It has been pointed out that the Ca in peat can be derived from underground water systems too (Chai, 1993), which could be an important source of Ca and related elements in sub-alpine karst regions. The acidic depositional environment of peat deposits is difficult for the forming of authigenic carbonate, making the sharp increases in mineral

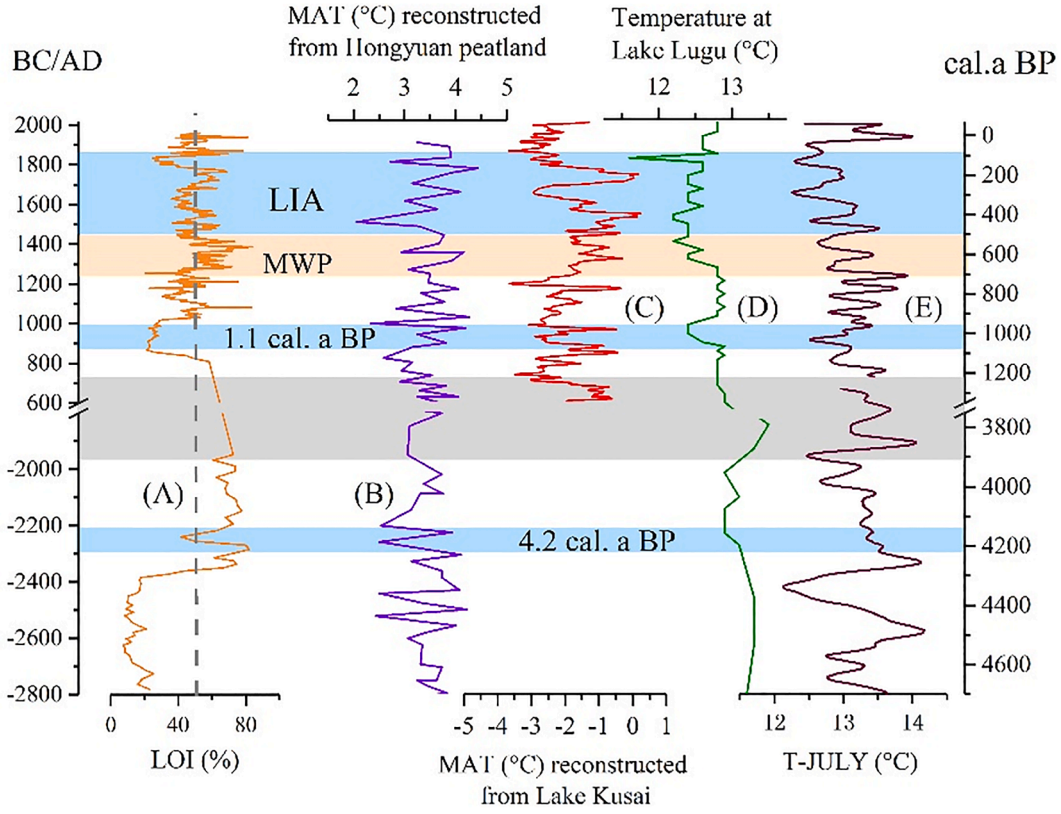

Fig. 6. Comparison of LOI in the Yejiping peat with other relevant records. (A) LOI in YJP01, (B) reconstructed MAT from the HY4 core of Hongyuan peatland (Yan et al., 2021), (C) reconstructed MAT variability at the Lake Kusai (Cui et al., 2021), the red line is the average of the 6-windows running, (D) BrGDGTs-inferred temperature of Core LG10 sediment from Lake Lugu (Zhao et al., 2020), (E) reconstructed summer (July) temperature record from the Scandinavian Peninsula (Helama et al., 2012). The brown line is the average of 33-windows running. The gray shaded part indicates discontinuity of sediment. (For interpretation of the references to color in this figure legend, the reader is referred to the web version of this article.)

contents normally related to abrupt environment changes, such as volcanic eruptions (Shi et al., 2021). In the Yejiping peatland, almost all ionic Ca^{2+} and Mg^{2+} originate from the surrounding limestone and dolomite mountains (Fig. 1). Since most materials that enter the basin are at a relatively stable rate, the increases in $CaCO_3$ are thus usually related to intensified exogenous inputs. It has been reported that the chemical dissolution of limestone mountains can be strengthened by the intensified surface runoff and groundwater during wet periods (Kong et al., 2010). This increases in chemical dissolution can thus accelerate the migration of Ca^{2+} and Mg^{2+}. As a result, the contents of these ions in the surface runoff were increasing (Li et al., 2014). It is therefore plausible to make the hypothesis that the increases in carbonate contents in karst peat sediments such as the YJP01 peat core, are linked with intensified precipitation.

Our SEM results show that very little amount of Ca can be crystallized due to the acidic environment of the Yejiping peatland. Ca exists in peat normally as an ionic state. However, the sample during the MWP appears to be in a crystalline state (Fig. 5). It has been pointed out that Ca^{2+} and Mg^{2+} ions in peat can also combine with humic acid that in the form of complexes and chelates (Hakanson and Jansson, 1983; Lerman, 1978). Besides, morphological characteristics of the detrital minerals under SEM also show that the debris during the MWP was larger and rounder, suggesting enhanced precipitation and water transport capability was stronger (Fig. 4A, B).

Although the Ca values that measured by the XRF scanning are slightly differed from the conventional $CaCO_3$ measurements, these two independent pair of measurements exhibited a general similar variation trend (Fig. 7A, B). The changes in $CaCO_3$, Ca, Fe_2O_3, LOI, and L* were synchronizing with each other (Fig. 3). In peat deposit, organic matter includes humus and plant residues (Chai, 1993). Less decomposed plant residues will contribute significantly bright components to the peat deposit, thus increasing its L* (Fig. 3D). Increases in L* were synchronized with enhanced precipitation, which will cause higher peat water content and peatland water table level. Which in turn contributes to less plant residue decomposition due to the anoxic environment. Therefore, LOI, L*, Ca, and $CaCO_3$ were relatively low during periods when the precipitation in SW China decreased (Fig. 3).

Three prominent cold events, 4200 cal. a BP, 950–1100 cal. a BP, and the LIA, were recorded in SW China by the Ca, $CaCO_3$, a* records in our reconstruction (Figs. 3, 6, 7). Additionally, the MWP warm period was clearly observed. $CaCO_3$ and Ca values decreased significantly at the bottom of the YJP01 core (from 4300 to 4100 cal. a BP), while the fluctuations in Fe_2O_3 values were relatively stable (Fig. 3A, E). Ca content decreased from 14.41 to 9.04, while the mean value of LOI was ~41% (Fig. 3C), indicating a cold climate during this period. The 4200 a BP cold event lasted for about 300 years in our YJP01 record. This cold event also corresponds with the enrichments of stalagmite $\delta^{18}O$ in the Dongge Cave in Guizhou Province (Fig. 7C) and the low SC_2 values in the sediments of Ximenglongtan in Yunnan Province, suggesting a dry SW China during this period (Fig. 7D).

All the environmental indicators fluctuated significantly during 950–1100 cal. a BP (Fig. 3). Ca decreased from 16.04 to 7.24 and $CaCO_3$ decreased from 1.76 to 1.22%. In the meantime, LOI rapidly decreased to 21.75% (Fig. 3A–C, E). On the contrary, L* only experienced slight decreases (Fig. 3A, C, D). It has been suggested that overly humid anoxic environments inhibit microbial activity (Chai, 1993). This could have been the reason for the observed decreases in humification and increases in L* (Fig. 3D). It has been reported that the decreases in humidity may promote the decomposition of microorganisms, which in turn increases the degree of peat humification in the overly humid environment in the western Guizhou Plateau (Yang et al., 2019). Therefore, the observed decreases in Ca, Mg, $CaCO_3$, and L* were related to cold and dry

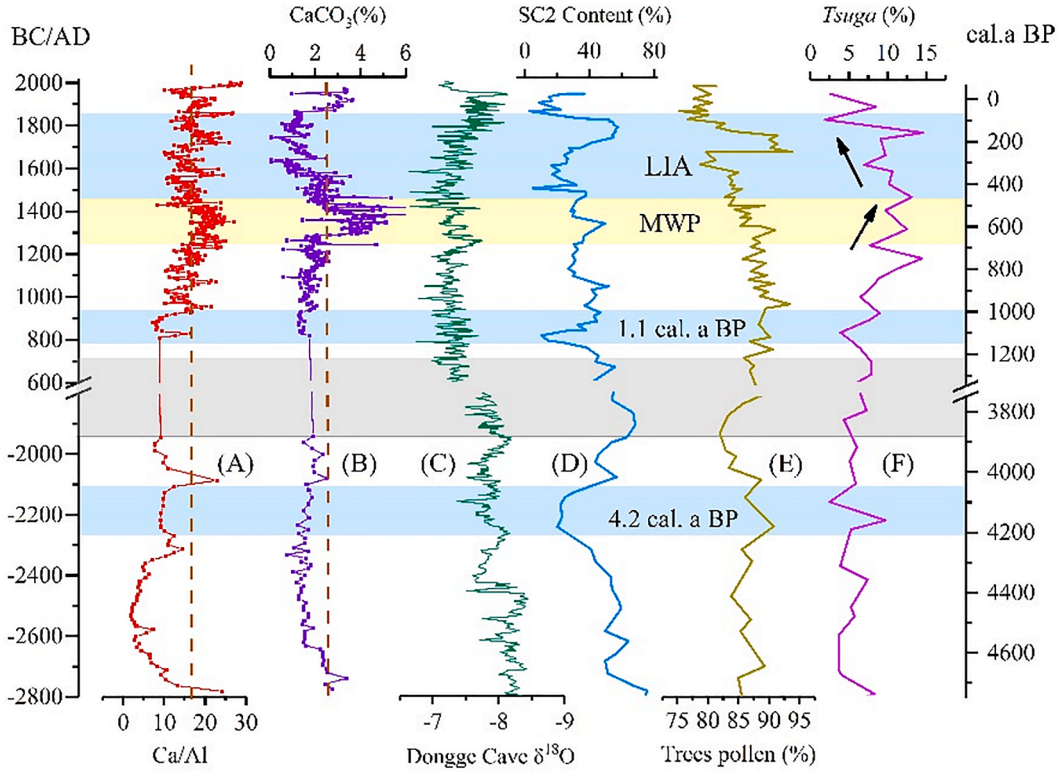

Fig. 7. Changes in the main indices of Yejiping peat and precipitation records over the past 4700 years. (A) Ca (red line) and (B) $CaCO_3$ content in YJP01, (C) $\delta^{18}O$ of DA stalagmite from Dongge Cave (Wang et al., 2005), (D) SC2 content extracted from the grainsize, which is a proxy for transportation power and precipitation in the sediments of Lake Ximenglongtan in Yunnan Province, southwestern China (Ning et al., 2017). (E) Tree pollen content in the pollen assemblage of Lake Lugu in the Yunnan Province, southwestern China (Wang et al., 2016), and (F) *Tsuga* pollen content in the pollen assemblage of Lake Erhai in the Yunnan Province, southwestern China (Dearing et al., 2008). (For interpretation of the references to color in this figure legend, the reader is referred to the web version of this article.)

climates. Reduced precipitation may have led to the peatland being more inclined to an oxidizing environment. Low LOI may reflect the decrease in temperature and thus signify a cold event. The low tree pollen content in Lake Lugu in Yunnan Province, SW China (Fig. 7E), also shows a dry and cold climate during 950–1100 cal. a BP. The high SC_2 value in the nearby Lake Ximenglongtan (Fig. 7D), also indicates less precipitation in this period. A cold event during this period has also been recorded by the MAT reconstruction by a peat core taken from the Hongyuan peatland (Fig. 6B) (Yan et al., 2021; Zeng et al., 2017). In addition, a sudden drop in the *Tsuga* pollen content in the pollen assemblage was observed in the sediment core taken from Lake Erhai (Fig. 7F) (Dearing et al., 2008). This also suggests a prominent dry climate in SW China during this period.

The two prominent cold-dry events in SW China at around ~4200 and ~1100 cal. a BP, which were clearly recorded by the LOI, Ca and $CaCO_3$ contents in the YJP01 peat core. Our reconstruction was consistent with the results of paleoclimatic reconstructions in other parts of the Yunnan–Guizhou Plateau as well as other regions controlled by the Indian monsoon (Dykoski et al., 2005; Ning et al., 2017; Wang et al., 2005) (Fig. 7B–D, Fig. 7C–F). Additionally, both the Guliya ice core and the Dulan tree ring records show that the Northern Hemisphere has become significantly warmer since the beginning of the 20th century (Yao et al., 2001). This is in line with our reconstruction using carbonate contents of the YJP01 core. The high-resolution climatic characteristics of the LIA and the MWP in SW China are discussed in the following subsection.

5.2. Detailed climatic evolutionary processes of the LIA and the MWP

5.2.1. MWP: 313–194 cm, 1200–1450 CE

Increases in Ca and $CaCO_3$ contents at the beginning of the MWP indicate enhanced precipitation (Fig. 7A, B). Meanwhile, the increases in LOI indicate a higher organic matter content and temperature during the MWP (Fig. 6A). However, Ca, $CaCO_3$, and LOI showed rapid declines at ~1250 CE following a brief increase (Fig. 6A, Fig. 7A, B). The occurrence of a short cold and dry period at the beginning of the MWP has also been recorded as the enrichment of $\delta^{18}O$ in the Dongge Cave stalagmite, which then bounced back after the climatic transition period (Fig. 7C). After this short interval, the environmental indicators of the YJP01 core rebounded rapidly and fluctuated at higher values (Fig. 3). An intensified precipitation in SW China during this period was also observed in the depletion in Dongge Cave stalagmite $\delta^{18}O$ (Fig. 7C). The variations in the characteristics of our analysis showed increased precipitation and temperature during the MWP (Figs. 3, 6, 7).

The temperature index of Lake Tiancai, northwest of Yunnan Province, shows that the climate was relatively warm during 800–1400 CE (Feng et al., 2019). A warm climate was also observed in the Yangzonghai basin in central Yunnan during 780–1630 CE (Yu et al., 2020). However, the LOI of the YJP01 core shows that the temperature in the Yejiping area was relatively lower during 800–1000 CE (Fig. 6A). After 1000AD, the temperature began to rise and was kept at a high level from 1250 to 1450 CE (corresponding to the depth at 295–194 cm, Fig. 6A). The temperature showed a significantly fluctuating and general ascending trend during 1000–1400 CE. The temperature during 1250–1450 CE was the highest, and variations in the precipitation showed an increase trend, like the temperature. The color of the peat that formed during this interval is mainly dark brown, which is lighter than the upper and lower layers (Fig. 2). Lots of plant residues can be observed in this layer, indicating that these peats are less decomposed. It can also be inferred that vegetation was abundant during the deposition, and the temperature and precipitation must be high enough to promote this high peat production. Plant residues normally decompose much slower in anoxic environments. We thus contend that 1250–1450 CE may have been the warmest and wettest period of SW China during the MWP (Fig. 7C).

The contents in Ca, $CaCO_3$, and LOI showed a significant decrease at ~1450 CE. This suggests that the climate has changed from warm-wet to cold-dry. Abundant plant residue was observed below 200 cm in the peat strata compared to that above 200 cm (the depth of 200 cm roughly corresponds to 1450 CE) (Fig. 2). This suggests that the transition from the MWP to the LIA may have occurred at ~1450 CE. The MWP recorded in the Yejiping peat, which was began at ~1200 CE and continued until 1450 CE, lasting ~250 years. While in our reconstruction, the MWP lasted from 950 to 1250 CE, which is different from that was defined in the fifth IPCC report (Stocker et al., 2013). Compared with the reconstructed temperature anomaly of China (Ge et al., 2013), the MWP in Yejiping may have lasted shorter and started later. The variations in the Ca counts of the YJP01 core are similar to the $\delta^{18}O$ ratio of the Dongge Cave stalagmite (Fig. 7C). It should be noticed that another stalagmite record from the Longquan Cave in south Guizhou Province has also revealed that the late stage of the MWP was between 1300 and 1550 CE (Zhang et al., 2009). This indicates that the climate in SW China during the MWP was prominently humid. However, a warm-dry MWP and cold-wet LIA have been shown in the lacustrine records of Lake Erhai, Lake Lugu, and Lake Yangzonghai (Yu et al., 2020). The differences in the spatial differentiation in the interior of SW China may have significantly impacted the dynamics in the climate evolution processes during the MWP.

5.2.2. LIA: 194–42 cm, 1450–1880 CE

As the last abrupt cooling event of the Holocene, the climate during the LIA fluctuated significantly and was clearly recorded in our YJP01 core and other archives in the world (Fig. 8). Both carbonate contents and LOI were low during the LIA, indicating relatively low precipitation and temperature during 1450–1880 CE (Fig. 8A, D). High $\delta^{18}O$ values in stalagmites from both the Jhumar Cave in central India (Sinha et al., 2011) and the Dongge Cave in SW China (Zhao et al., 2021) were observed during this period (Fig. 8B, C), suggesting that the climate of both East Asia and South Asia during the LIA was significantly drier than that during the MWP. With an average sedimentation rate of 2.8 years/cm, the YJP01 peat core has a high temporal resolution during this period. This provides an opportunity for comprehending the detailed hydroclimate evolution of the LIA. In our reconstruction, the LIA can be further divided into six sub-intervals, namely sub-interval 1, 2, 3, 4, 5, and 6 (Fig. 8). These sub-intervals were closely related to the precipitation (Fig. 8B, C), SC2 content, trees and *Tsuge* pollen content in Fig. 7D–F, and the temperature records (Fig. 6B–E, 8E–J), and solar activity (Fig. 8K).

5.2.2.1. Sub-interval 1 (1450–1560 CE). The LOI during this interval was lower than that of the MWP and fluctuated significantly at an average of ~50% (Fig. 8D). Ca values were relatively low and showed a general decreasing trend (Fig. 8A). $\delta^{18}O$ of the stalagmite from the Jhumar Cave was higher during this period (Fig. 8B), while that of the Dongge Cave slightly decreased at the beginning (Fig. 8C). Alkenone-inferred summer lake surface temperature (SLST) records from Lake Gahai sediments in the QTP (He et al., 2013) (Fig. 8G) and the reconstructed temperature anomaly of SW China showed descending trends during this interval (Fig. 8H), while that of the Northern Hemisphere was relatively low too (Fig. 8J). This suggests that the climate of SW China was cold and dry during 1450–1550 (or 1420–1570) AD, which corresponds to the Spele minimum period (Wilfried, 2001). The decreases in temperature observed in the YJP01 core could also be attributed to the low solar activity during this interval (Fig. 8K).

5.2.2.2. Sub-interval 2 (1560–1620 CE). Ca in the YJP01 core increased slightly and then decreased during this sub-interval (Fig. 8A), indicating an initial increase in the precipitation but later was decreasing. The stalagmite from the Jhumar Cave was enriched in $\delta^{18}O$ during this period (Fig. 8B), while the Dongge Cave stalagmite has recorded the highest $\delta^{18}O$values (Fig. 8C). This suggests the precipitation in the

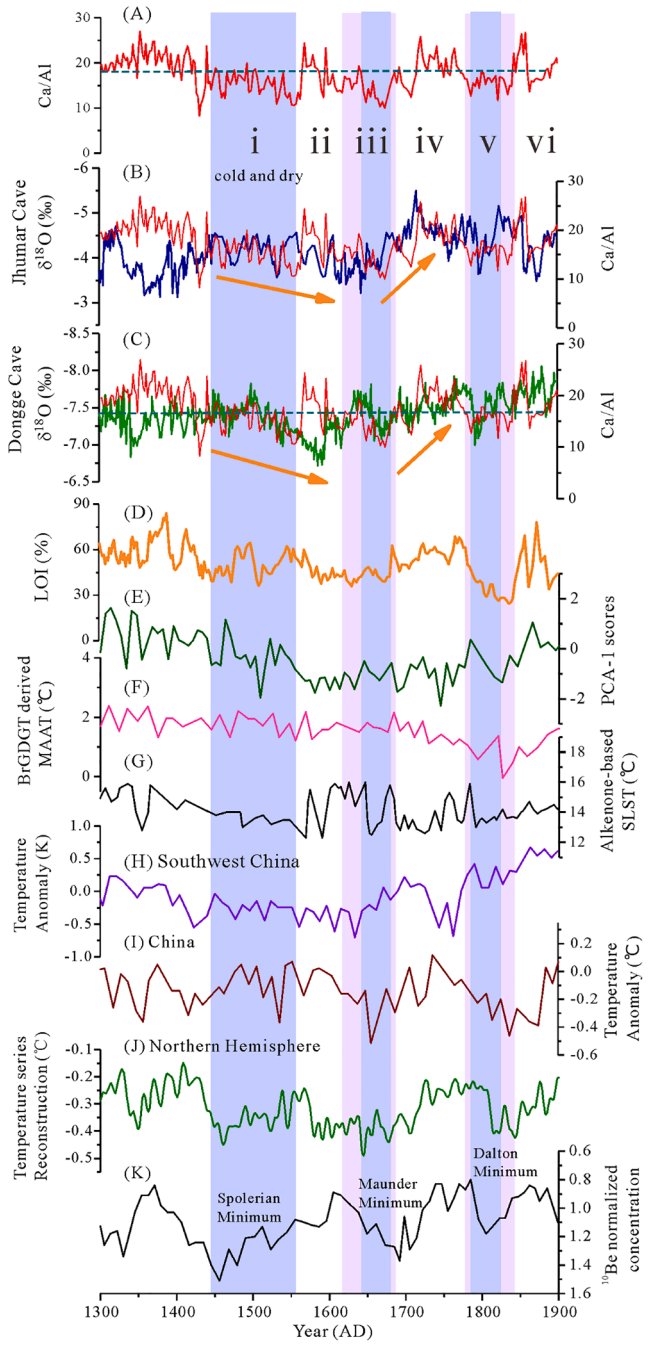

Fig. 8. Changes in Ca content and LOI in the Yejiping peat during the LIA, and their comparison with other records from previous studies. (A) Ca content in the YJP01 core, (B) $\delta^{18}O$ of Jhumar Cave in central India (Sinha et al., 2011), (C) $\delta^{18}O$ of DX1 from Dongge Cave (Zhao et al., 2015), (D) LOI in the YJP01 core, (E) sample scores for the first principal component analysis (PCA1) of pollen taxa in Basomtso sediments from the southeast of the QTP (Li et al., 2017a, 2017b). (F) branched glycerol dialkyl glycerol tetraethers (BrGDGT) derived MAAT (°C) from Lake Tiancai in Yunnan Province, southwestern China (Feng et al., 2019), (G) alkenone-inferred summer lake surface temperature (SLST) records from Lake Gahai in the QTP (He et al., 2013), (H) reconstructed temperature anomaly of Southwest China (Kuang et al., 2011), (I) reconstructed temperature anomaly of China (Ge et al., 2013), (J) reconstructed temperature series of the Northern Hemisphere (Mann et al., 2009) and (K) ^{10}Be stack (variations relative to the 843–1876 CE average) (Delaygue and Bard, 2011).

regions that were dominated by the Indian Monsoon during this period was the lowest compared to the other LIA sub-intervals. The LOI (average 42%) of the YJP01 core decreased significantly in this sub-interval (Fig. 8D). The significantly decreased sample scores for the first principal component analysis (PCA1) of pollen taxa from Lake Basomtso sediments from the southeast of the QTP, revealing low temperature (Fig. 8E) (Li et al., 2017a, 2017b). Meanwhile, the reconstructed temperature anomaly of both the SW China (Fig. 8H) and the Northern Hemisphere (Fig. 8J) was lower than in the previous sub-interval. It is thus can be deduced that the climate of SW China at the interval 1560–1620 CE was dry and cold.

5.2.2.3. Sub-interval 3 (1620–1670 CE). Ca and $CaCO_3$ decreased significantly from 1620 to 1670 CE (Fig. 7A, B). In the meantime, $\delta^{18}O$ values of the stalagmite from the Dongge Cave (Fig. 8C) also showed a descending trend, reflecting a decrease in precipitation. Besides, significant decreases were observed in the temperature anomalies of both China and the Northern Hemisphere, and also the summer lake surface temperature reconstructed from Lake Gahai on the QTP (Fig. 8G, I, J). However, the LOI in the YJP01 core and the reconstructed temperature anomaly in SW China (Fig. 8D, H) showed that the temperature did not decrease significantly during this interval. The temperature in SW China was similar to that of the previous interval, with an increase in the degree of drought. Interestingly, this cold-dry climate was linked with the solar minimum, known as the Maunder minimum, lasting from 1640 to 1670 CE. The enriched $\delta^{18}O$ of the stalagmite in the Jhumar Cave also indicates that precipitation in South Asia at sub-interval 3 may have been at its lowest during the LIA (Fig. 8B). Furthermore, the $\delta^{18}O$ and $\delta^{13}C$ values in the XY07-8 stalagmite from the Xinya Cave, Chongqing, also indicate a dry SW China at around 1650 CE (Li et al., 2017a, 2017b).

5.2.2.4. Sub-interval 4 (1670–1780 CE). Ca at sub-interval 4 increased and reached its maximum during the LIA (Fig. 8A). In the meantime, stalagmites from both Dongge and Jhumar caves showed significant depletion in $\delta^{18}O$ during this time, reaching their minimum since the beginning of the LIA (Fig. 8B, C). This indicates that the precipitation in these three sites significantly increased during this interval. Besides, the reconstructed annual temperature from Lake Basomtso, the SLST reconstructed from Lake Gahai sediments in the QTP, the temperature anomaly in SW China and the whole China, and the reconstructed temperature in the Northern Hemisphere were high during this time interval (Fig. 8E, G–J). We contend that the climate of SW China in this interval is the warmest and wettest during the LIA.

5.2.2.5. Sub-interval 5 (1780–1840 CE). During 1790–1820 CE, Ca values in the YJP01 core dropped significantly, while the $\delta^{18}O$ values of the stalagmite from the Dongge and Jhumar caves showed an increasing trend (Fig. 8A–C). Meanwhile, a rapid decrease in organic matters was observed during this interval (Fig. 8D). The reconstructed temperature anomaly in China, the Northern Hemisphere (Fig. 8I, J) and other sites from the QTP and southwestern China all basically decreased during this interval (Fig. 8E–G), indicating a cold climate at sub-interval 5. Unlike the increase in precipitation after 1820 CE, which was indicated by the depleted $\delta^{18}O$ of stalagmites from the Jhumar and Dongge caves (Fig. 8B, C). We observed a cold and dry climate during 1820–1840 CE in the Yejiping peatland. This cold and dry period corresponds to the 1790–1830 CE low solar activity period (Fig. 8K), which is also known as the Dalton Minimum. During 1780–1810 CE, the $\delta^{18}O$ values of the stalagmite from the Heizhugou Cave in Sichuan Province, SW China, also increased significantly (Jiang et al., 2017). This pattern was also observed in the Omani stalagmite $\delta^{18}O$ (Fleitmann et al., 2003), the Dasop ice core on the northern slope of the Himalayas in China (Thompson, 2000), and the Asian tree-ring record (Matzel et al., 2010). Furthermore, an anomalous increase in the $\delta^{13}C$ values of $CaCO_3$ during 1788–1881 CE was observed in the Caohai in the west Guizhou Plateau.

This also indicates a cold SW China during this interval (Zhu et al., 2013).

5.2.2.6. Sub-interval 6 (1840–1880 CE). The increases in Ca and LOI in the YJP01 core indicate a rising temperature and precipitation in SW China during this stage (Fig. 8A, D). The reconstructed temperature anomaly in China and the average temperature anomaly in southwestern China and other regions also showed similar increases in temperature (Fig. 8E–J). For example, the higher values of PCA1 of pollen taxa from Lake Basomtso sediments in the QTP (Fig. 8E) and the branched glycerol dialkyl glycerol tetraethers (BrGDGT) derived MAAT (°C) from Lake Tiancai sediments in Yunnan Province (Feng et al., 2019) (Fig. 8F), all indicated prominent increases in temperature. Our analysis shows that the detailed hydroclimate changes during the LIA have been recorded in the YJP01 core.

5.3. Controls and mechanisms of hydroclimatic changes in the western Guizhou Plateau over the past 4700 years

The changes in contents of the YJP01 core Ca and $CaCO_3$ can reflect the intensity of precipitation and thus are closely related to the variation in the intensity of the Indian monsoon (Figs. 7, 8). This pattern has also been reported in previous studies (Wang et al., 2010). The changes in temperature, which were indicated by the variations in LOI, were consistent with the temperature trends across regions controlled by the Indian monsoon (Figs. 6, 8). In addition, Ca content and LOI (Fig. 9A, B) were closely related to the El Niño Southern Oscillation (ENSO) events (Fig. 9C) and the climate reconstructed by the ^{10}Be stack (Fig. 9F). The driving forces of the Asian monsoon during the late Holocene, such as solar radiation, Atlantic meridional overturning circulation (AMOC), and the Intertropical Convergence Zone (ITCZ) (Yang et al., 2010), are discussed below.

The main quasi-periods on decadal-to-centennial timescales that observed in the YJP01 core were 500, 125, 103, 80, 58, 43, 40, 38, 30, 27, 25, 20, and 12a (Fig. 5). Among these quasi-periods, 500, 125, and 80a are close to the 572, 116, and 77a quasi-periods recorded in the Nantun peat total mercury concentrations (Niu et al., 2017). It is worth noting that a 512a quasi-period has also been observed in the global tree ring ^{14}C ratios (Stuiver and Braziunas, 1993). Furthermore, the 500 and 80a cycles are also close to the 475 and 77a cycles that were observed in the δ^{13}C values of the Hongyuan peat in the northeast of the QTP (Hong et al., 2004). Besides, the 80a cycle also corresponds to the 76a climate

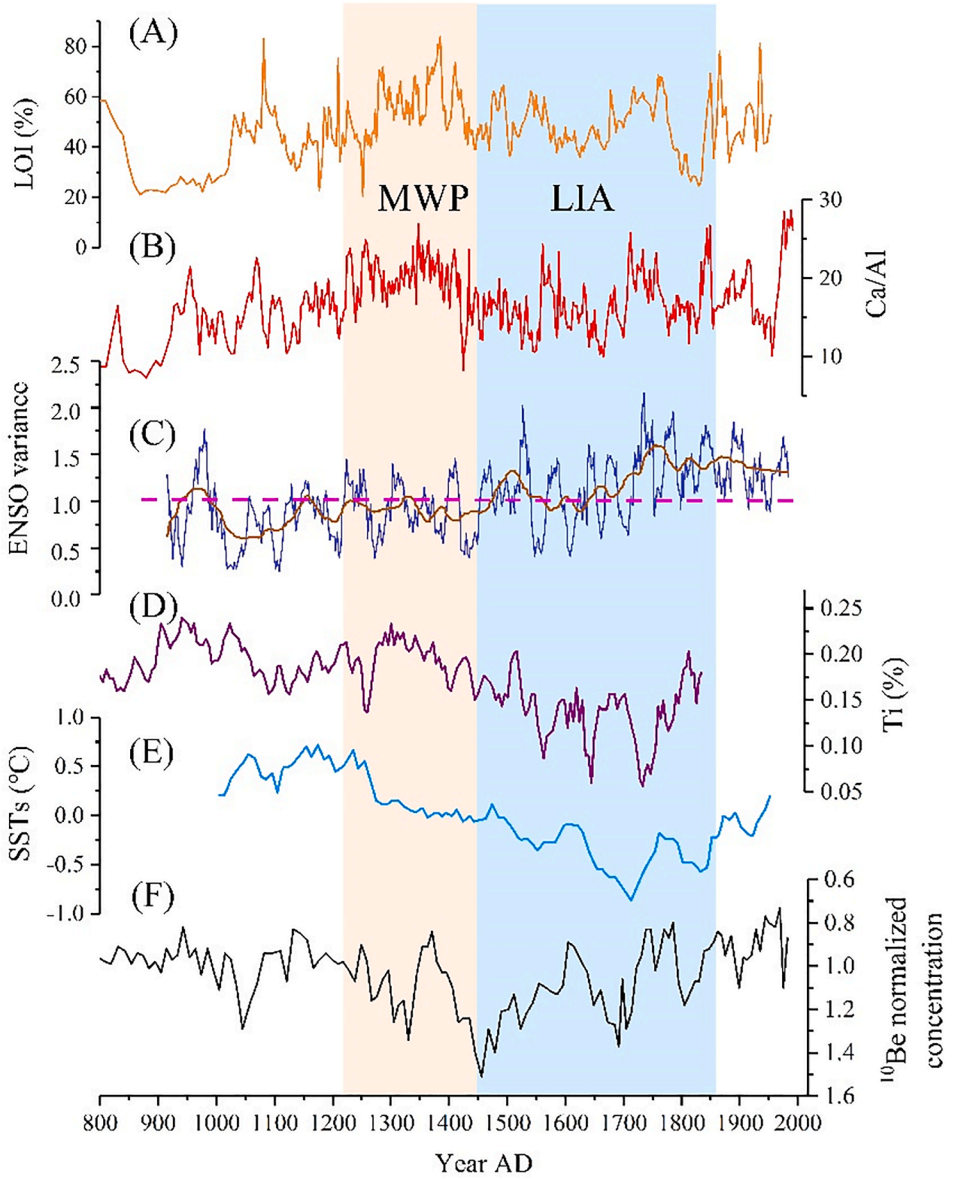

Fig. 9. Comparisons of Ca content and LOI in the Yejiping peat with El Niño Southern Oscillation (ENSO) and solar activities since the LIA. (A) LOI and (B) Ca content (red line) in the YJP01 core, (C) ENSO variance (Li et al., 2011), (D) Ti concentration from the anoxic Cariaco Basin, revealing ITCZ migrations (Haug et al., 2001). (E) Sea surface temperature (SST) records from the tropical Indo-Pacific warm pool (Oppo et al., 2009), and (F) ^{10}Be stack (variations relative to the 843–1876 CE average) (Delaygue and Bard, 2011). (For interpretation of the references to color in this figure legend, the reader is referred to the web version of this article.)

cycle of the North Atlantic (Schlesinger and Ramankutty, 1994). The 103a cycle corresponds to the century cycle in solar activity, known as the Gleissberg period.

The 58a period observed in the YJP01 core was consistent with the 50–70a inter-decadal period of the Pacific Decadal Oscillation Index (PDO) (MacDonald and Case, 2005). While the 52-58a cycle was close to the 55a solar cycle (Fleitmann et al., 2003) and also the 60a cycle that was recorded in the stalagmites of Hulu Cave in Nanjing, eastern China (Wu et al., 2006). It has been suggested that the 60a solar cycle has a direct influence on the intensity of the Indian summer monsoon (Agnihotri et al., 2002). Besides, the 52a cycle has been observed in the ~3000-year paleo-flood events reconstruction in the Jianghan Plain in central China, which was controlled by the Asian monsoon (Xie et al., 2007). The prominent 24a and 39a cycles, which were related to solar activity, are also observed in the analysis of the Dulan tree-ring record from the northeast of the QTP (Kang et al., 1997). The 25a, 38a, and 40a cycles observed in the YJP01 core were close to that observed in the Dulan tree ring. The quasi-periods of 20a and 12a may also be related to the Haie (22a) and Schwabe (11a) solar activity cycles (Richard and Hugh, 1991; Tsiropoula, 2003). Moreover, the analyses on $\delta^{18}O$ of the Guliya ice core, glacier accumulation rates, and the Qilian Mountain tree-ring record (Yao et al., 2001) have also confirmed the existence of this 22a cycle.

On the millennial timescale, solar radiation at 30°N continued to weaken since the early Holocene. It has been reported that the ^{10}Be stack was higher during MWP than the LIA (Fig. 9F). It has been suggested that the warm climate in the MWP was mainly caused by strong solar radiation based on the simulation of the global air-sea coupling model (Delaygue and Bard, 2011). The air temperature of the Northern Hemisphere was higher during the MWP (Mann et al., 2009). The ENSO variance decreased during the MWP (Li et al., 2011), showing a La Niña-like state (Fig. 9C). Corresponding to the northward migration of the ITCZ during the MWP (Fig. 9D), the temperature in the western Pacific warm pool was abnormally increasing (Fig. 9E) and the Walker circulation was intensifying (Trenberth and Caron, 2000; Yan et al., 2011). This leads to an increase in precipitation in the region controlled by the Indian Monsoon. Ca contents of the YJP01 core reveal that SW China has experienced abundant precipitation during the MWP. While influenced by the AMOC downdraft, the climate of the east coast of the Pacific Ocean appeared to be dry during this period (Kennett et al., 2012).

There existed three solar minimum periods in the LIA, namely the Spele minimum (1450–1550 CE), Mundell minimum (1645–1715 CE), and Dalton Minimum (1790–1830 CE). These abrupt decreases in solar activities were well recorded in the YJP01 peat core (Fig. 9A, B). As solar radiation weakened, the decreases in both the Cariaco Basin sediment core Ti contents (Haug et al., 2001) (Fig. 9D) and the YJP01 peat core LOI (Fig. 8A) indicate that the ITCZ migrated southward during the LIA (Li et al., 2011). Besides, a prominent El Niño state (Mann et al., 2005) (Fig. 9C) and a weaker Walker circulation (Yan et al., 2011) were also observed during this period. This leads to a weakening Indian monsoon (Krishna et al., 1999; Kumar et al., 2006, 1999), which then caused a decrease in precipitation in SW China during the LIA (Fig. 9B). The decreases in precipitation in the early 16th and late 18th centuries that recorded in the YJP01 core and stalagmites in the Indian monsoon regions may be caused by the strong El Niño events (Fig. 9C, D) and low sea surface temperature in the tropical Indo-Pacific warm pool (Fig. 9E). This is in line with previous studies suggesting that regional precipitation was weakened during several strong ENSO periods (Ming et al., 2020).

The variations in Indian Ocean monsoon intensities during the LIA that recorded in the YJP01 peat core, just as the reconstruction in the nearby Yunnan Province indicated, were strongly linked with the ocean–atmosphere cycles in the Indo-Pacific (Zhao et al., 2021). Solar activities have a very strong influence on the intensities of the Indian monsoon by acting on the global ocean–atmosphere coupling system. This may have been the most important driving force for the observed changes in temperature and precipitation in SW China. As the fluctuation in the ENSO variance was increasing from the MWP to the LIA, the climate of the Indian Ocean monsoon region was expected to transform from a La Niña state to an El Niño state. We thus suggest that the weakening Indian Ocean monsoon may be the main reason that the regional climate in SW China has changed from the MWP warm-wet to the LIA cold-dry.

6. Conclusions

We conducted systematic investigations on the organic matter and carbonate contents of a karst depression peat core in the western Guizhou Plateau, SW China. High carbonated as well as Ca contents are linked with warm and humid climates. The hydroclimate fluctuations reconstructed by Ca-related indicators in the YJP01 core were consistent with records from SW China and other regions controlled by the Indian monsoon. Abrupt climate changes at 4.2 ka, 1.1 ka, the MWP, and the LIA were clearly observed in our reconstruction. Benefitting from its high temporal resolution and peat carbonate contents being very sensitive to hydrological changes, our reconstruction shows that the LIA can be divided into six intervals. In addition, we found 500, 125, 103, 80, 58, 43, 20, and 12-a quasi-periods in the carbonate contents of the YJP01 core, corresponding to the Gleissberg, Haie, Schwabe, and PDO cycles. Our reconstruction has a great potential to provide a better understanding of the paleoenvironmental significance of Ca-related indices in peat sediments in karst regions.

CRediT authorship contribution statement

Mengxiu Zeng: Conceptualization, Methodology, Funding acquisition, Writing – original draft, Writing – review & editing, Visualization. **Qiao Zeng:** Investigation, Resources, Writing – original draft, Writing – review & editing, Visualization. **Haijun Peng:** Conceptualization, Methodology, Funding acquisition, Writing – original draft, Writing – review & editing, Visualization. **Yongqiu Wu:** Conceptualization, Methodology, Funding acquisition. **Yue Li:** Investigation, Resources. **Yougui Song:** Investigation, Resources. **Enguo Sheng:** Investigation, Resources. **Yangyang Wu:** Investigation, Resources. **Tianyang Wang:** Investigation, Resources. **Jian Ni:** Conceptualization, Methodology, Funding acquisition, Investigation, Resources.

Declaration of Competing Interest

The authors declare that they have no known competing financial interests or personal relationships that could have appeared to influence the work reported in this paper.

Acknowledgments

This study was supported by the National Natural Science Foundation of China (Grant Nos: 42007400, 41773140, and 41971111), the National Key Research and Development Project of China (2016YFC0502101), and the Science and Technology Foundation of Guizhou Province (Grant Nos: [2020]1Y193 and [2019]1317).

References

Agnihotri, R., Dutta, K., Bhushan, R., Somayajulu, B.L.K., 2002. Evidence for solar forcing on the Indian monsoon during the last millennium. Earth Planet. Sc. Lett. 198, 521–527.

Anderson, W.T., Mullins, H.T., 1997. Stable isotope record from Seneca Lake, New York: Evidence for a cold paleoclimate following the Younger Dryas. Geology 25, 135–138.

Bhattacharya, F., Shukla, A.D., Patel, R.C., Rastogi, B.K., Juyal, N., 2017. Sedimentology, geochemistry and OSL dating of the alluvial succession in the northern Gujarat alluvial plain (western India) - A record to evaluate the sensitivity of a semiarid fluvial system to the climatic and tectonic forcing since the late Marine Isotopic Stage 3. Geomorphology 297, 1–19.

Blaauw, M., Christen, J.A., 2011. Flexible paleoclimate age-depth models using an Autoregressive Gamma Process. Bayesian Anal. 6, 457–474.
Cambardella, C.A., Gajda, A.M., Doran, J.W., Wienhold, B.J., Kettler, T.A., 2001. Estimation of particulate and total organic matter by weight loss-on-ignition. In: Lal, R. (Ed.), Assessment Methods for Soil Carbon. Adv. Soil Sci. CRC Press, Boca Raton, pp. 349–359.
Chai, X., 1993. Peatland. Geological Publishing House, Beijing in Chinese.
Chen, C., Yuan, D., Cheng, H., Yu, T., Shen, C., Edwards, R.L., Wu, Y., Xiao, S., Zhang, J., Wang, T., Huang, R., Liu, Z., Li, T., Li, J., 2021. Human activity and climate change triggered the expansion of rocky desertification in the karst areas of Southwestern China. Sci. China Earth Sci. 64, 1761–1773.
Chen, W., Ren, M., Lu, Z., Wang, N., 2010. Research on the property of soil geochemistry in typical karst area in Guizhou Province. Carsologica Sinica 3, 246–252 in Chinese with English abstract.
Chen, X., Fang, X., An, Z., Han, W., Wang, X., Bai, Y., Hong, Y., 2007. An 8.1Ma calcite record of Asian summer monsoon evolution on the Chinese central Loess Plateau. Sci. China Ser. D: Earth Sci. 50, 392–403.
Cui, A.N., Lu, H.Y., Liu, X.Q., Shen, C.M., Xu, D.K., Xu, B.Q., Wu, N.Q., 2021. Tibetan Plateau Precipitation Modulated by the Periodically Coupled Westerlies and Asian Monsoon. Geophys. Res. Lett. 48 e2020GL091543.
Cui, A.N., Ma, C.M., Zhao, L., Tang, L.Y., Jia, Y.L., 2018. Pollen records of the Little Ice Age humidity flip in the middle Yangtze River catchment. Quatern. Sci. Rev. 193, 43–53.
Dai, C., Chen, J., Wang, X., 2014. The Guizhou geological map series and integrative study on geology in Guizhou Province—A new vision of "Guizhou Regional Geology". Manage. Res. Sci. Technol. Achiev. 50–55 in Chinese with English abstract.
Dearing, J.A., Jones, R.T., Shen, J., Yang, X., Boyle, J.F., Foster, G.C., Crook, D.S., Elvin, M.J.D., 2008. Using multiple archives to understand past and present climate-human-environment interactions: the lake Erhai catchment, Yunnan Province, China. J. Paleolimnol. 40, 3–31.
Delaygue, G., Bard, E., 2011. An Antarctic view of Beryllium-10 and solar activity for the past millennium. Clim. Dynam. 36, 2201–2218.
Deng, X., Bi, K., 2004. Analysis on the Karst topographic distribution in Guizhou Province. Guizhou Geol. 21 (191–193), 177 in Chinese with English abstract.
Dixit, Y., Tandon, S.K., 2016. Hydroclimatic variability on the Indian subcontinent in the past millennium: Review and assessment. Earth-Sci. Rev. 161, 1–15.
Dykoski, C.A., Edwards, R.L., Cheng, H., Yuan, D., Cai, Y., Zhang, M., Lin, Y., Qing, J., An, Z., Revenaugh, J., 2005. A high-resolution, absolute-dated Holocene and deglacial Asian monsoon record from Dongge Cave, China. Earth Planet. Sc. Lett. 233, 71–86.
Fan, J.W., Xiao, J.L., Wen, R.L., Zhang, S.R., Huang, Y., Yue, J.J., Wang, X., Cui, L.L., Li, H., Xue, D.S., Liu, Y., 2019. Mineralogy and carbonate geochemistry of the Dali Lake sediments: Implications for paleohydrological changes in the East Asian summer monsoon margin during the Holocene. Quatern. Int. 527, 103–112.
Fang, X.M., Li, J.J., Edward, D., Ewart, A.F., Rob, A.K., 1994. Micromorphology of the Beiyuan loess-paleosol sequence in Gansu Province, China: geomorphological and paleoenvironmental significance. Palaeogeogr. Palaeoclimatol. Palaeoecol. 111, 289–303.
Feng, X.P., Zhao, C., D'Andrea, W.J., Liang, J., Zhou, A.F., Shen, J., 2019. Temperature fluctuations during the Common Era in subtropical southwestern China inferred from brGDGTs in a remote alpine lake. Earth Planet. Sc. Lett. 510, 26–36.
Fleitmann, D., Burns, S.J., Mudelsee, M., Neff, U., Kramers, J., Mangini, A., Matter, A., 2003. Holocene forcing of the Indian monsoon recorded in a stalagmite from southern Oman. Science 300, 1737–1739.
Gao, Y., Xiong, K.N., Quan, M.Y., Song, B., Peng, H.J., Peng, H.R., Shen, W.D., Bao, K.S., 2019. Holocene climate dynamics derived from pollen record of Jiulongchi wetland in Fanjing Mountain, southwest China. Quatern. Int. 513, 1–7.
Ge, Q., Liu, J., Fang, X., Yang, B., Hao, Z., Shao, X., Zheng, J., 2013. General characteristics of temperature change and centennial warm periods during the past 2000 years. Acta Geogr. Sin. 68, 579–592 in Chinese with English abstract.
Gong, X., Chen, C., Tang, Y., Huang, K., Yue, Y., Liang, K., Zheng, Z., 2019. Palaeoenvironment changes during the past 21 ka inferred from organic geochemical records of Caohai Lake, Guizhou Province. J. Palaeogeogr. 21, 1025–1034 in Chinese with English abstract.
Grieman, M.M., Aydin, M., McConnell, J.R., Saltzman, E.S., 2018. Burning-derived vanillic acid in an Arctic ice core from Tunu, northeastern Greenland. Clim. Past 14, 1925–1937.
Hadad, M.A., Gonzalez-Reyes, A., Roig, F.A., Matskovsky, V., Cherubini, P., 2021. Tree-ring-based hydroclimatic reconstruction for the northwest Argentine Patagonia since 1055 CE and its teleconnection to large-scale atmospheric circulation. Global Planet. Change 202, 103496.
Hakanson, L., Jansson, M., 1983. Principles of Lake Sedimentology. Springer, Berlin-Verlag.
Han, J., Keppens, E., Liu, T., Paepe, R., Jiang, W., 1997. Stable isotope composition of the carbonate concretion in loess and climate change. Quatern. Int. 37, 37–43.
Hans, J., 1980. The Soil Resource. Springer, New York.
Haug, G.H., Hughen, K.A., Sigman, D.M., Peterson, L.C., Röhl, U., 2001. Southward migration of the intertropical convergence zone through the Holocene. Science (New York N.Y.) 293, 1304–1308.
He, Y., Liu, W., Zhao, C., Wang, Z., Wang, H., Liu, Y., Qin, X., Hu, Q., An, Z., Liu, Z., 2013. Solar influenced late Holocene temperature changes on the northern Tibetan Plateau. Chinese Sci. Bull. 58, 1053–1059.
Heiri, O., Lotter, A.F., Lemcke, G., 2001. Loss on ignition as a method for estimating organic and carbonate content in sediments: reproducibility and comparability of results. J. Paleolimnol. 25, 101–110.
Helama, S., Seppä, H., Bjune, A.E., Birks, H.J., 2012. Fusing pollen-stratigraphic and dendroclimatic proxy data to reconstruct summer temperature variability during the past 7.5 ka in subarctic Fennoscandia. J. Paleolimnol. 48, 275–286.
Hillman, A.L., O'Quinn, R.F., Abbott, M.B., Bain, D.J., 2020. A Holocene history of the Indian monsoon from Qilu Lake, southwestern China. Quatern. Sci. Rev. 227, 106051.
Hong, B., Lin, Q., Hong, Y., Zhu, Y., Wang, Y., Leng, X., 2004. Evolution of Southwest Monsoon in the eastern part of Qinghai-Tibet Plateau during Holocene. Earth Environ. 32, 42–49 in Chinese with English abstract.
Huang, W., Tu, Y., 1983. Vegetation regionalization in Guizhou. J. Guizhou Normal Univ. (Natural Sci.) 26–47 in Chinese with English abstract.
Jiang, W., Zhao, K., Chen, S., Wang, Y., Cheng, H., Ning, Y., 2017. Decadal climate oscillations during the Little Ice Age of stalagmite record from Heizhugou Cave, Sichuan. Quatern. Sci. 37, 118–129 in Chinese with English abstract.
Kang, X.C., Graumlich, L.J., Sheppard, P., 1997. The last 1835 years climate changes inferred from tree ring records in Dulan region, Qinghai, China. Quatern. Sci. 70–75. In Chinese with English abstract.
Kaniewski, D., Van Campo, E., Paulissen, E., Weiss, H., Bakker, J., Rossignol, I., Van Lerberghe, K., 2011. The medieval climate anomaly and the little Ice Age in coastal Syria inferred from pollen-derived palaeoclimatic patterns. Global Planet. Change 78, 178–187.
Kennett, D.J., Breitenbach, S.F.M., Aquino, V.V., Asmerom, Y., Awe, J., Baldini, J.U.L., Bartlein, P., Culleton, B.J., Ebert, C., Jazwa, C., Macri, M.J., Marwan, N., Polyak, V., Prufer, K.M., Ridley, H.E., Sodemann, H., Winterhalder, B., Haug, G.H., 2012. Development and Disintegration of Maya Political Systems in Response to Climate Change. Science 338, 788–791.
Konen, M.E., Jacobs, P.M., Burras, C.L., Talaga, B.J., Mason, J.A., 2002. Equation for predicting soil organic carbon using loss-on-ignition for north central U.S. soils. Soil Sci. Soc. Am. J. 66, 1878–1881.
Kong, F., Yang, R., Han, X., Wei, H., Cheng, M., Gao, J., Ren, H., Long, J., 2011. Analysis of sediment provenanace and sedimentary control factors in Yaoshang Formation, Weining County in Guizhou Province. Geoscience 25, 464–475 in Chinese with English abstract.
Kong, F., Yang, R., Lin, S., 2010. Analysis of evolution of Karst environment of Weining Region, Guizhou Province, West China: A proof from the sediment evolution of Lake Caohai since about 73 Million Years. Earth Environ. 38, 138–145 in Chinese with English abstract.
Krishna, K.K., Rajagopalan, B., Cane, M.A., 1999. On the weakening relationship between the Indian monsoon and ENSO. Science 284, 2156–2159.
Kuang, X., Liu, J., Wang, H., Ti, R., 2011. Comparison of simulated and reconstructed temperature in China during the last Millennium. Quatern. Sci. 31, 48–56 in Chinese with English abstract.
Kumar, K.K., Rajagopalan, B., Hoerling, M., Bates, G., Cane, M., 2006. Unraveling the mystery of Indian monsoon failure during El Nino. Science 314, 115–119.
Kumar, K.K., Rajagopalan, B., Cane, M.A., 1999. On the Weakening Relationship Between the Indian Monsoon and ENSO. Science 284, 2156–2159.
Lerman, A., 1978. Lakes: Chemistry, Geology, Physics. Springer-Verlag, New York.
Li, J.B., Xie, S.P., Cook, E.R., Huang, G., D'Arrigo, R., Liu, F., Ma, J., Zheng, X.T., 2011. Interdecadal modulation of El Nino amplitude during the past millennium. Nat. Clim. Change 1, 114–118.
Li, J.Y., Li, H.C., Li, T.Y., Mii, H.S., Yu, T.L., Shen, C.C., Xu, X.M., 2017a. High-resolution $\delta^{18}O$ and $\delta^{13}C$ records of an AMS^{14}C and $^{230}Th/U$ dated stalagmite from Xinya Cave in Chongqing: Climate and vegetation change during the late Holocene. Quatern. Int. 447, 75–88.
Li, K., Liu, X.Q., Wang, Y.B., Herzschuh, U., Ni, J., Liao, M.N., Xiao, X.Y., 2017b. Late Holocene vegetation and climate change on the southeastern Tibetan Plateau: Implications for the Indian Summer Monsoon and links to the Indian Ocean Dipole. Quatern. Sci. Rev. 177, 235–245.
Li, R., Gao, J., Zhang, L., Li, J., Ji, H., 2014. Element geochemical characteristics of red weathering crust from dolomite, north Guizhou, China. Carsol. Sin. 33, 396–404 in Chinese with English abstract.
Li, X., 2001. Evolution of karst geomorphology of upper-Cenozoic and its influential factors in Guizhou Plateau. Guizhou Geol. 18, 29–36 in Chinese with English abstract.
Lopez-Aviles, A., Garcia-Alix, A., Jimenez-Moreno, G., Anderson, R.S., Toney, J.L., Mesa-Fernandez, J.M., Jimenez-Espejo, F.J., 2021. Latest Holocene paleoenvironmental and paleoclimate reconstruction from an alpine bog in the Western Mediterranean region: The Borreguil de los Lavaderos de la Reina record (Sierra Nevada). Palaeogeogr. Palaeocl. 573, 110434.
Löwemark, L., Chen, H.F., Yang, T.N., Kylander, M., Yu, E.F., Hsu, Y.W., Lee, T.Q., Song, S.R., Jarvis, S., 2011. Normalizing XRF-scanner data: A cautionary note on the interpretation of high-resolution records from organic-rich lakes. J. Asian Earth Sci. 40, 1250–1256.
Lu, Y., 1981. Pleistocene climatic cycles and variation of CaCO3 contents in a loess profile. Scientia Geologica Sinica 122–131. In Chinese with English abstract.
MacDonald, G.M., Case, R.A., 2005. Variations in the Pacific Decadal Oscillation over the past millennium. Geophys. Res. Lett. 32, L08703.
Mann, M.E., Cane, M.A., Zebiak, S.E., Clement, A., 2005. Volcanic and Solar Forcing of the Tropical Pacific over the past 1000 Years. J. Climate 18, 447–456.
Mann, M.E., Zhang, Z.H., Rutherford, S., Bradley, R.S., Hughes, M.K., Shindell, D., Ammann, C., Faluvegi, G., Ni, F.B., 2009. Global Signatures and Dynamical Origins of the Little Ice Age and Medieval Climate Anomaly. Science 326, 1256–1260.
Matzel, J.E.P., Ishii, H.A., Joswiak, D., Hutcheon, I.D., Bradley, J.P., Brownlee, D., Weber, P.K., Teslich, N., Matrajt, G., McKeegan, K.D., MacPherson, G.J., 2010. Constraints on the formation age of Cometary Material from the NASA Stardust Mission. Science 328, 483–486.

Manoj, M.C., Thakur, B., Uddandam, P.R., 2021. Controls on rare earth elements distribution from Kerala coast, southwest India over the past 2000 years. Environ. Forensics 1–16.
Mikhailova, A.B., Grenaderova, A.V., Kurina, I.V., Shumilovskikh, L.S., Stojko, T.G., 2021. Holocene vegetation and hydroclimate changes in the Kansk forest steppe, Yenisei River Basin, East Siberia. Boreas 50, 948–966.
Ming, G.D., Zhou, W.J., Cheng, P., Wang, H., Xian, F., Fu, Y.C., Wu, S.G., Du, H., 2020. Lacustrine record from the eastern Tibetan Plateau associated with Asian summer monsoon changes over the past similar to 6 ka and its links with solar and ENSO activity. Clim. Dynam. 55, 1075–1086.
Mullins, H.T., 1998. Environmental change controls of lacustrine carbonate, Cayuga Lake, New York. Geology 26, 443–446.
Nazarova, L.B., Razjigaeva, N.G., Golovatyuk, L.V., Biskaborn, B.K., Grebennikova, T.A., Ganzey, L.A., Mokhova, L.M., Diekmann, B., 2021. Reconstruction of Environmental Conditions in the Eastern Part of Primorsky Krai (Russian Far East) in the Late Holocene. Contemp. Probl. Ecol. 14, 218–230.
Ning, D.L., Zhang, E.L., Sun, W.W., Chang, J., Shulmeister, J., 2017. Holocene Indian Summer Monsoon variation inferred from geochemical and grain size records from Lake Ximenglongtan, southwestern China. Palaeogeogr. Palaeoclimatol. Palaeoecol. 487, 260–269.
Niu, R., Zhou, L., Meng, Q., Wang, L., Sun, C., Liu, T., Wang, Z., Zheng, X., 2017. The paleoclimate variations of the Nantun peat in the Caohai area since the Middle Holocene. Quatern. Sci. 37, 1357–1369 in Chinese with English abstract.
Njagi, D.M., Routh, J., Olago, D., Gayantha, K., 2021. A multi-proxy reconstruction of the late Holocene climate evolution in the Kapsabet Swamp, Kenya (East Africa). Palaeogeogr. Palaeoclimatol. Palaeoecol. 574, 110475.
Oppo, D.W., Rosenthal, Y., Linsley, B.K., 2009. 2,000-year-long temperature and hydrology reconstructions from the Indo-Pacific warm pool. Nature 460, 1113–1116.
Quamar, M.F., Bera, S.K., 2021. A 8400-year pollen records of vegetation dynamics and Indian Summer Monsoon climate from central India: Signatures of global climatic events. J. Palaeontol. Soc. Ind. 66, 12–22.
Quan, M., Gao, Y., Xiong, K., Lu, Y., Shen, W., 2019. Paleoclimate change of the Fanjingshan World Natural Heritage Property since Holocene. Earth Environ. 47, 610–620 in Chinese with English abstract.
Richard, C.W., Hugh, S.H., 1991. The Sun's luminosity over a complete solar cycle. Nature 351, 42–44.
Rudaya, N., Nazarova, L., Frolova, L., Palagushkina, O., Soenov, V., Cao, X., Syrykh, L., Grekov, I., Otgonbayar, D., Bayarkhuu, B., 2021. The link between climate change and biodiversity of lacustrine inhabitants and terrestrial plant communities of the Uvs Nuur Basin (Mongolia) during the last three millennia. Holocene 31, 1443–1458.
Schlesinger, M.E., Ramankutty, N., 1994. An oscillation in the global climate system of period 65–70 years. Nature 367, 723–726.
Sachs, J.P., Muegler, I., Sachse, D., Prebble, M., Wolhowe, M., 2021. Last millennium hydroclimate in the central equatorial North Pacific (5 degrees N, 160 degrees W). Quatern. Sci. Rev. 259, 106906.
Shi, G., Yan, H., Zhang, W.C., Dodson, J., Heijnis, H., 2021. The impacts of volcanic eruptions and climate changes on the development of Hani peatland in northeastern China during the Holocene. J. Asian Earth Sci. 210, 104691.
Silliman, J.E., Meyers, P.A., Bourbonniere, R.A., 1996. Record of postglacial organic matter delivery and burial in sediments of Lake Ontario. Org. Geochem. 24, 463–472.
Sinha, A., Berkelhammer, M., Stott, L., Mudelsee, M., Cheng, H., Biswas, J., 2011. The leading mode of Indian Summer Monsoon precipitation variability during the last millennium. Geophys. Res. Lett. 38, L15703.
Stocker, T.F., Qin, D., Plattner, G.K., Midgley, P.M., 2013. Climate Change 2013: The physical science basis. Contribution of Working Group I to the Fifth Assessment Report of the Intergovernmental Panel on Climate Change, IPCC 2013.
Stuiver, M., Braziunas, T.F., 1993. Modeling atmospheric ^{14}C influences and ^{14}C ages of Marine Samples to 10,000 BC. Radiocarbon 35, 137–189.
Thompson, L.G., 2000. Ice core evidence for climate change in the Tropics: implications for our future. Quatern. Sci. Rev. 19, 19–35.
Trenberth, K.E., Caron, J.M., 2000. The Southern Oscillation Revisited: Sea Level Pressures, Surface Temperatures, and Precipitation. J. Climate 13, 4358–4365.
Tripathi, S., Basumatary, S.K., Pandey, A., Khan, S., Tiwari, P., Thakur, B., 2021. Palaeoecological changes from 580 to 1220 CE from the Indo-Burma region: A biotic assessment from the Barak Valley of Assam, northeast India. Catena 206, 105487.
Tsiropoula, G., 2003. Signatures of solar activity variability in meteorological parameters. J. Atmos. Sol-Terr. Phy. 65, 469–482.
van Bellen, S., Garneau, M., Booth, R.K., 2011. Holocene carbon accumulation rates from three ombrotrophic peatlands in boreal Quebec, Canada: Impact of climate-driven ecohydrological change. Holocene 21, 1217–1231.
Wang, H., Hong, Y.T., Lin, Q.H., Hong, B., Zhu, Y.X., Wang, Y., Xu, H., 2010. Response of humification degree to monsoon climate during the Holocene from the Hongyuan peat bog, eastern Tibetan Plateau. Palaeogeogr. Palaeoclimatol. Palaeoecol. 286, 171–177.
Wang, Q., Yang, X.D., Anderson, N.J., Dong, X.H., 2016. Direct versus indirect climate controls on Holocene diatom assemblages in a sub-tropical deep, alpine lake (Lugu Hu, Yunnan, SW China). Quatern. Res. 86, 1–12. In Chinese with English abstract.
Wang, X., Wang, L., Hu, S., Ma, M., Wang, Q., Cui, B., Zhan, C., Zeng, L., Liu, X., Shen, J., 2021a. Indian summer monsoon variability over last 2000 years inferred from sediment magnetic characteristics in Lugu Lake, southwest China. Palaeogeogr. Palaeocl. 578, 110581.
Wang, Y., Cheng, H., Edwards, R.L., He, Y., Kong, X., An, Z., Wu, J., Kelly, M.J., Dykoski, C.A., Li, X., 2005. The Holocene Asian monsoon: links to solar changes and North Atlantic climate. Science 308, 854–857.
Wang, Y., Liu, X., Han, L., Ni, Z., Ma, X., Wei, Y., Li, Z., 2021b. Late Holocene climate variation on the northern Tibetan Plateau inferred from Lake Ayakum. Catena 207, 105599.
Wilfried, S., 2001. Comment on the paper "Possible links between the solar radius variations and the Earth's climate evolution over the past four centuries". J. Atmos. Sol-Terr. Phy. 63, 2003.
Wu, J., Shao, X., Kong, X., Wang, Y., 2006. Imprint of solar activity on Nanjing stalagmite annual layer thickness sequence during the Last Glacial Maximum. Sci. Bull. 51, 431–435 in Chinese with English abstract.
Wu, X., Shen, J., Wang, Y., 2011. Holocene paleoenvironmental evolution of the Huguangyan Maar Lake. Mar. Geol. Quatern. Geol. 31, 155–162 in Chinese with English abstract.
Xiao, X.Y., Haberle, S.G., Shen, J., Yang, X.D., Han, Y., Zhang, E.L., Wang, S.M., 2014. Latest Pleistocene and Holocene vegetation and climate history inferred from an alpine lacustrine record, northwestern Yunnan Province, southwestern China. Quatern. Sci. Rev. 86, 35–48.
Xie, Y., Li, C., Wang, Q., Yin, H., 2007. Sedimentary records of paleoflood events during the last 3000 years in Jianghan Plain. Scientia Geographica Sinica 27, 81–84 in Chinese with English abstract.
Yan, H., Sun, L.G., Oppo, D.W., Wang, Y.H., Liu, Z.H., Xie, Z.Q., Liu, X.D., Cheng, W.H., 2011. South China Sea hydrological changes and Pacific Walker Circulation variations over the last millennium. Nat. Commun. 2, 293.
Yan, T.L., Zhao, C., Yan, H., Shi, G., Sun, X.S., Zhang, C., Feng, X.P., Leng, C.C., 2021. Elevational differences in Holocene thermal maximum revealed by quantitative temperature reconstructions at similar to 30 degrees N on eastern Tibetan Plateau. Palaeogeogr. Palaeoclimatol. Palaeoecol. 570, 110364.
Yang, H., Zeng, M.X., Peng, H.J., Li, K., Li, F., Zhu, L., Deng, B., Liao, M.N., Ni, J., 2020. Application of XRF core scanning method in Late Holocene environment change study derived from a peat core from southwestern Guizhou, Southwestern China. Quatern. Sci. 40, 1154–1169 (in Chinese with English abstract).
Yang, Y., Yuan, D., Cheng, H., Zhang, M., Tan, J., Lin, Y., Zhu, X., Edwards, R.L., 2010. Precise dating of abrupt shifts in the Asian monsoon during the last deglaciation based on stalagmite data from Yamen Cave, Guizhou province, China. Sci. China Earth Sci. 40, 199–210 in Chinese with English abstract.
Yang, Y., Zhang, D., Lan, B., Abdusalih, N., Feng, Z., 2019. Peat $\delta^{13}C_{celluose}$-signified moisture variations over the past ~2200 years in the southern Altai Mountains, northwestern China. J. Asian Earth Sci. 174, 59–67.
Yao, T., Yang, M., Kang, X., 2001. Comparative study of the climate changes in the past 2000 years by using ice core and tree ring records. Quatern. Sci. 21, 514–519 in Chinese with English abstract.
Yu, X., Zeng, H., Huang, L., Sun, Q., Wang, M., Zhang, H.C., Shen, C., 2020. Environmental changes over the past 1200 years in the catchment of Yangzonghai Lake, Central Yunnan. Chinese J. Ecol. 39, 1896–1910 in Chinese with English abstract.
Zeng, M., Zhu, C., Song, Y., Ma, C., Yang, Z., 2017. Paleoenvironment change and its impact on carbon and nitrogen accumulation in the Zoige wetland, northeastern Qinghai-Tibetan Plateau over the past 14,000 years. Geochem. Geophy. Geosy. 18, 1775–1792.
Zhang, C., Wu, S., 2020. An analysis on moisture source of extreme precipitation in summer Southwest China. J. Natural Resour. 1–12 in Chinese with English abstract.
Zhang, E.L., Chang, J., Sun, W.W., Cao, Y.M., Langdon, P., Cheng, J., 2018. Potential forcings of summer temperature variability of the southeastern Tibetan Plateau in the past 12 ka. J. Asian Earth Sci. 159, 34–41.
Zhang, L., Ji, H., Gao, J., Li, R., Li, J., 2015. Geochemical characteristics of major, trace and rare earth elements in typical carbonate weathered profiles of Guizhou Plateau. Geochimica 44, 323–336 in Chinese with English abstract.
Zhang, M., Cheng, H., Lin, Y., Qin, J., Zhu, X., Ran, J., Yang, Y., Chen, H., Edwards, R.L., 2006. High-resolution climatic record from a stalagmite in the past 2000 years in Libo, Guizhou Provience. Acta Sedimentol. Sin. 24, 339–348 in Chinese with English abstract.
Zhang, M., Zhu, X., Cheng, H., Lin, Y., Qin, J., Ran, J., Wang, H., He, S., 2009. A high resolution paleoclimate record of the last 1,200 years in stalagmite L2 from the Longquan Cave, Guizhou Province. Acta Geoscientica Sinica 30, 831–840 in Chinese with English abstract.
Zhao, C., Rohling, E.J., Liu, Z.Y., et al., 2020. Possible obliquity-forced warmth in southern Asia during the last glacial stage. Sci. Bull. 66, 1136–1145.
Zhao, C., Cheng, J., Wang, J.J., et al., 2021. Paleoclimate significance of reconstructed rainfall isotope changes in Asian monsoon region. Geophys. Res. Lett. 48 (12) e2021GL092460.
Zhao, K., Wang, Y.J., Edwards, R.L., Cheng, H., Liu, D.B., Kong, X.G., 2015a. A high-resolved record of the Asian Summer Monsoon from Dongge Cave, China for the past 1200 years. Quatern. Sci. Rev. 122, 250–257.
Zhao, M., Li, H.C., Liu, Z.H., Mii, H.S., Sun, H.L., Shen, C.C., Kang, S.C., 2015b. Changes in climate and vegetation of central Guizhou in southwest China since the last glacial reflected by stalagmite records from Yelang Cave. J. Asian Earth Sci. 114, 549–561.

Zheng, J., Bian, J., Ge, Q., Hao, Z., Yin, Y., Liao, Y., 2013. The climate regionalization in China for 1981–2010. Chinese Sci. Bull. 58, 3088–3099 in Chinese with English abstract.
Zheng, Q., Zhang, H., Ming, Q., Chang, F., Meng, H., Zhang, W., Liu, M., Shen, C., 2014. Vegetational and environmental changes since 15ka B.P. recorded by lake Lugu in the southwest monsoon domain region. Quatern. Sci. 34, 1314–1326 in Chinese with English abstract.
Zhu, Z.J., Chen, J.A., Zeng, Y., 2013. Abnormal positive $\delta^{13}C$ values of carbonate in Lake Caohai, southwest China, and their possible relation to lower temperature. Quatern. Int. 286, 85–93.